DUDLEY KNOX LIBRARY
NAVAL POSTGRADUATE SCHOOL
MONTEREY, CALIFORNIA 93943

NAVAL POSTGRADUATE SCHOOL
Monterey, California

THESIS

FIBER OPTIC GRADIENT HYDROPHONE

by

Gary B. Mills

June 1984

Thesis Advisor: E. F. Carome

Approved for public release; distribution unlimited

T211554

REPORT DOCUMENTATION PAGE		READ INSTRUCTIONS BEFORE COMPLETING FORM
1. REPORT NUMBER	2. GOVT ACCESSION NO.	3. RECIPIENT'S CATALOG NUMBER
4. TITLE (and Subtitle) Fiber Optic Gradient Hydrophone		5. TYPE OF REPORT & PERIOD COVERED Master's Thesis June 1984
		6. PERFORMING ORG. REPORT NUMBER
7. AUTHOR(s) Gary B. Mills		8. CONTRACT OR GRANT NUMBER(s) N0001483WR30294 N0001484WR24017
9. PERFORMING ORGANIZATION NAME AND ADDRESS Naval Postgraduate School Monterey, California 93943		10. PROGRAM ELEMENT, PROJECT, TASK AREA & WORK UNIT NUMBERS
11. CONTROLLING OFFICE NAME AND ADDRESS Naval Postgraduate School Monterey, California 93943		12. REPORT DATE June 1984
		13. NUMBER OF PAGES 109
14. MONITORING AGENCY NAME & ADDRESS(if different from Controlling Office)		15. SECURITY CLASS. (of this report)
		15a. DECLASSIFICATION/DOWNGRADING SCHEDULE

16. DISTRIBUTION STATEMENT (of this Report)

Approved for public release; distribution unlimited

17. DISTRIBUTION STATEMENT (of the abstract entered in Block 20, if different from Report)

18. SUPPLEMENTARY NOTES

19. KEY WORDS (Continue on reverse side if necessary and identify by block number)

fiber optic sensor, hydrophone, gradient, acoustic calibrator, Mach-Zehnder interferometer, pressure gradient hydrophone, phase modulation, feedback stabilization, interferometric sensor.

20. ABSTRACT (Continue on reverse side if necessary and identify by block number)

A laboratory study has been made of the characteristics of an interferometric type optical fiber pressure gradient hydrophone. The optical system is configured as an all-fiber Mach-Zehnder interferometer excited by a single mode gallium arsenide diode laser. A pair of identical fiber coils, one in each arm of the interferometer, forms the sensing portion of the gradient hydrophone. Each coil consists of 10 meters of polyethylene jacketed, single mode fiber, wound in a doughnut shaped element of mean diameter 4 cm and thickness 3 mm. An acoustic calibrator, similar in design to the USRD type G40 shipboard calibrator used by the U.S. Navy, was constructed for use in obtaining single and dual (dipole) coil sensitivities. The acoustic sensitivity of each coil was determined separately and then the pair was aligned coaxially and separated by 10 cm to operate as a pressure gradient device. Details of the construction of the system, calibration procedure, lock-in demodulator, and hydrophone sensitivity data are presented. The system has demonstrated a 14 dB sensitivity advantage over the USRD type G63 standard (piezoelectric) pressure gradient hydrophone.

Approved for Public Release, Distribution Unlimited.

Fiber Optic Gradient Hydrophone

by

Gary B. Mills
Lieutenant, United States Navy
B.S., University of Utah, 1975

Submitted in partial fulfillment of the
requirements for the degree of

MASTER OF SCIENCE IN ENGINEERING ACOUSTICS

from the

NAVAL POSTGRADUATE SCHOOL
June 1984

Thesis
M5943
c.1

ABSTRACT

A laboratory study has been made of the characteristics of an interferometric type optical fiber pressure gradient hydrophone. The optical system is configured as an all-fiber Mach-Zehnder interferometer excited by a single mode gallium arsenide diode laser. A pair of identical fiber coils, one in each arm of the interferometer, forms the sensing portion of the gradient hydrophone. Each coil consists of 10 meters of polyethylene jacketed, single mode fiber, wound in a doughnut shaped element of mean diameter 4 cm and thickness 3 mm. An acoustic calibrator, similar in design to the USRD type G40 shipboard calibrator used by the U.S. Navy, was constructed for use in obtaining single and dual (dipole) coil sensitivities. The acoustic sensitivity of each coil was determined separately and then the pair was aligned coaxially and separated by 10 cm to operate as a pressure gradient device. Details of the construction of the system, calibration procedure, lock-in demodulator, and hydrophone sensitivity data are presented. The system has demonstrated a 14 dB sensitivity advantage over the USRD type G63 standard (piezoelectric) pressure gradient hydrophone.

TABLE OF CONTENTS

I. INTRODUCTION 11

A. BACKGROUND 11

B. PURPOSE OF THE STUDY 13

C. FORMAT OF THE REPORT 16

II. THEORY 17

A. CONVENTIONAL GRADIENT HYDROPHONE 17

B. CALIBRATION OF GRADIENT HYDROPHONE 27

C. FIBER OPTIC ACOUSTIC SENSOR 29

1. Acoustically Induced Phase Modulation . . 29

2. Feedback Stabilization 35

III. EXPERIMENTAL APPARATUS 41

A. INTERFEROMETER DESIGN AND CONSTRUCTION 41

B. INTERFEROMETER COMPONENTS 44

1. Laser Source 44

2. Fiber Specifications 47

3. 3 dB Coupler 50

4. Piezoelectric Phase Shifter 52

5. Polarization Controller 52

6. Photodetector 52

C. FIBER PREPARATION AND SPLICING 53

D. INSTRUMENTATION AND DATA ACQUISITION 59

1. HP-85F Computer 59

2. Arbitrary Waveform Generator HP3314A . . . 60

3. Spectrum Analyzer HP3582A 60

4. Oscilloscope Tektronix 2215 61

5. Digital Multimeter HP 3438A 61

6. Standard Hydrophone LC-10 61

7. Acoustic Calibrator 62

8. Locking Circuit 69

IV. EXPERIMENTAL PROCEDURE AND RESULTS 70

A. INTERFEROMETER CHARACTERISTICS 70

B. INDIVIDUAL SENSOR SENSITIVITY 78

C. GRADIENT SENSOR SENSITIVITY 83

D. ANALYSIS 89

V. CONCLUSIONS AND RECOMMENDATIONS 94

APPENDIX A: DATA ACQUISITION PROGRAM 96

APPENDIX B: SAMPLE RAW DATA 99

LIST OF REFERENCES 104

BIBLIOGRAPHY 106

INITIAL DISTRIBUTION LIST 107

LIST OF TABLES

I. Sound Speed in Calibrator 65

II. Comparison of Experimental Data with Bessel Theory 77

III. Individual Coil Sensitivity 82

IV. Gradient Sensor Sensitivities 88

LIST OF FIGURES

1.1. Fiber Optic Interferometric Hydrophone 14

1.2. Fiber Optic Interferometric Gradient Hydrophone . 15

2.1. Directivity Pattern of Pressure Gradient Hydrophone 18

2.2. Geometry Used in Deriving Sensing Characteristics of Acoustic Dipole (Pressure Gradient) 20

2.3. Pressure Distribution as Function of Distance from Null Pressure Point 22

2.4. Pressure and Velocity Distribution in a Standing Wave Tube 24

2.5 Photodetector Output Current as Function of Phase Difference between Interferometric Arms . . 36

2.6 Phase-Locked Loop Homodyne Detection Circuit . . 38

3.1. Schematic of Experimental Interferometric System 42

3.2. Photograph of Experimental Interferometric System 45

3.3. Schematic of Laser Diode Power Supply 46

3.4. CW-234 Laser Diode Power Curve 48

3.5. CWX-233 Laser Diode Power Curve 49

3.6. ITT Single Mode Fiber T-1601 51

3.7. Clairex CLD-41 Relative Irradiation Curve 54

3.8. Representation of Proper and Improper Cleaves . . 57
3.9. Photograph of Acoustic Calibrator 63
3.10. Sectional View of Acoustic Calibrator 64
3.11. LC-10 Voltage in Calibrator at 391 Hz 66
3.12. LC-10 Voltage in Calibrator at 593 Hz 67
3.13. LC-10 Voltage in Calibrator at 753 Hz 68
4.1. Block Diagram of Instrumentation Setup 71
4.2. Oscillograms of PZT Drive Signal and Photodiode Output Signal 73
4.3. Bessel Function Behavior of Photodiode Output . . 74
4.4. Photograph of LC-10 Hydrophone and Single Fiber Coil Setup 79
4.5. Block Diagram of Calibration Circuit 80
4.6. Demodulated Gradient Hydrophone Output at 593 Hz 92
4.7. Demodulated Gradient Hydrophone Output at 752 Hz 93

ACKNOWLEDGEMENTS

I want to express my gratitude to those who, because of their support, assistance, and encouragement, have made the completion of this work possible. First of all I would like to acknowledge Dr. Edward F. Carome and Dr. Steven L. Garrett, my thesis advisor and thesis co-advisor. I am extremely grateful for their help and continual support throughout the months of research. Dr. Garrett's support and encouragement throughout my Master's program made the time definitely worthwhile and a very rewarding experience. Thank you Steve. I want to give special acknowledgement to Machinist Robert Moeller who manufactured and machined a major portion of the mechanical apparatus used. I appreciate the support of the Office of Naval Research which provided the funds for this project.

I wish to dedicate this work to my wife Karen, my son David, and my daughter Kristen. Without their full support and encouragement, total confidence, and all sharing love this project would never have been completed.

I. INTRODUCTION

A. BACKGROUND

The use of optical fibers for communication and sensing is a rapidly expanding area of recent technology. Optical fiber technology is a little over a decade old, starting with the first demonstrations of low-loss (less than 1000 dB/km) optical fiber waveguides. Technological advances in material processing, fabrication of optical fibers, interconnection devices, cables, sources, and detectors now allow repeaterless light transmission over great distances (tens of kilometers) with an extremely large bandwidth [Ref. 1].

Capitalizing on the availability of optical fiber components, there has been significant interest and progress in the past half decade in exploitation of optical fibers as transduction elements in a new class of sensors. These sensors are capable of detecting acoustic fields, linear and rotational acceleration, temperature, strain, electric and magnetic fields, and other physical parameters. This versatility can also lead to difficulties and much effort has been expended to enhance sensitivity to the parameter of interest while desensitizing the fiber to all other fluctuations [Ref. 2]. Fiber sensors offer a number of potential advantages: increased sensitivity, geometric versatility as fiber sensors can be configured in arbitrary shapes, lightweight components, and low cost. Progress in demonstrating these advantages has been substantial in the past few years with over 60 different types of sensors using optical fiber as the transduction element being developed. These sensors range from simple on/off fluid level indicators, to the more sophisticated interferometric configurations. This large number of individual devices is usually categorized into amplitude or phase sensors. In effect, the sensor modulates some parameter of the lightwave in an optical fiber, such as the intensity or the phase. In the former case the physical perturbation interacts with the fiber to directly modulate the intensity of the light in the fiber. In the latter case the physical perturbation modulates the optical phase of coherent light propagating through the fiber. Optical interferometry must be utilized to convert the optical phase modulation to optical intensity modulation in order to permit photodetection. This technique allows for extremely high sensitivity. Phase modulation, conversion of phase modulation to intensity by interferometry, and subsequent detection by photodiodes will be discussed in more detail in Chapter II.

B. PURPOSE OF THIS STUDY

Fiber optic acoustic sensors were first demonstrated to be feasible in 1977 [Ref. 3 and 4]. Since then a significant degree of progress has been achieved, both in the understanding of the relevant acousto-optic transduction mechanisms as well as in component development and sensor packaging [Ref. 5 and 6]. Most of the fiber optic hydrophone work performed to date has been with monopolar omnidirectional devices. Figure 1.1 illustrates the basic geometry of a typical fiber optic hydrophone which utilizes acoustically induced phase modulation for transduction. A laser beam is split into two arms of an interferometer where a sensing coil in one arm is exposed to the acoustic pressure field while a reference coil, forming the second arm, is isolated from the field. The two beams are recombined and allowed to interfere on the surface of a photodetector.

Since their invention in the late 1970's two unique characteristics of interferometric type fiber optic hydrophones, i.e., their basic two-arm design and their proven high sensitivity, have suggested their use as gradient-type devices. A fiber optic gradient hydrophone has a sensing coil in each arm of the interferometer and both are exposed to the pressure field. Figure 1.2 illustrates the basic geometry of an acoustic fiber optic

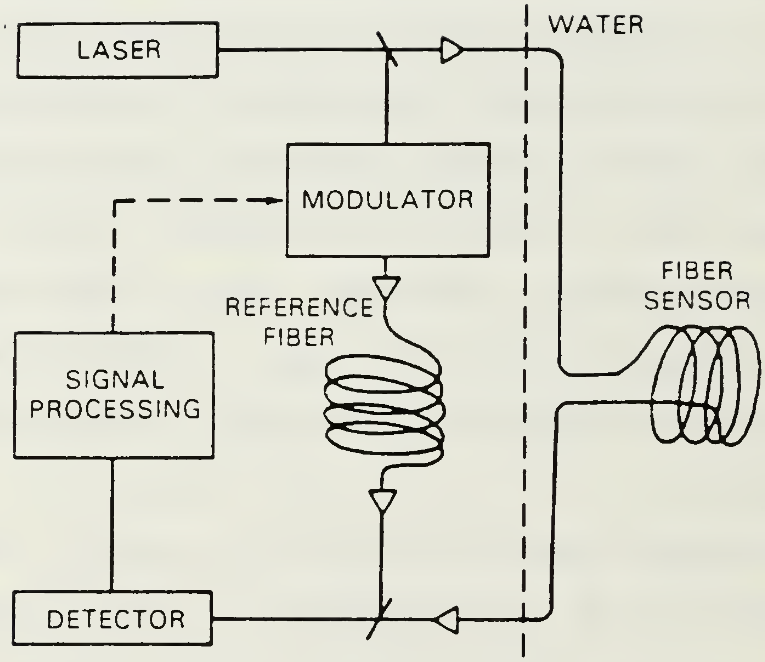

Figure 1.1 Fiber Optic Interferometric Hydrophone

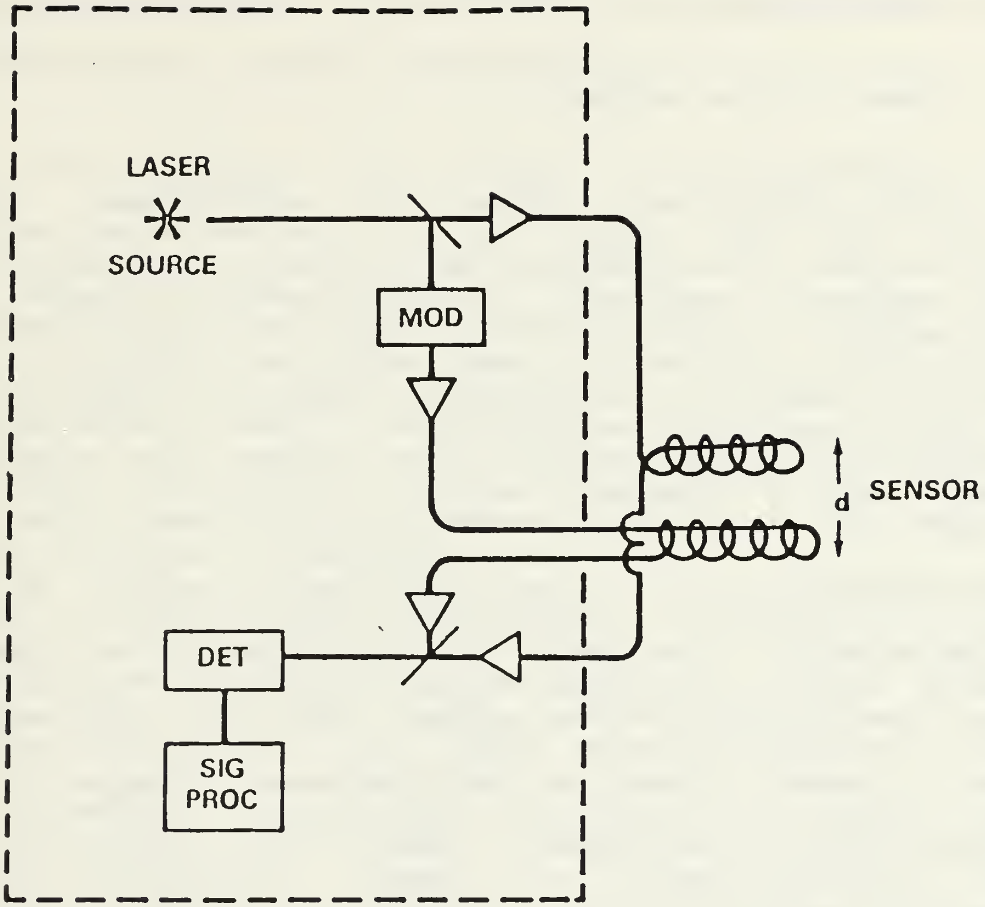

- BOTH SENSOR AND REFERENCE COIL INSONIFIED
- DETECTS SPATIAL VARIATION IN EXCITATION FIELD

Figure 1.2 Fiber Optic Interferometric Gradient Hydrophone

gradient hydrophone. It was the aim of this project to construct and partially evaluate in a laboratory environment the characteristics of a fiber optic gradient hydrophone.

C. FORMAT OF THE REPORT

The theoretical bases of conventional gradient hydrophones, the calibration of gradient hydrophones, and the behavior of interferometric sensors used in preparation of this report is presented in Chapter II. Details of the construction of the optical fiber sensor are presented in Chapter III. Included in Chapter III is a description of the characteristics of the individual parts of the interferometer. The parts are discussed in the order that they were built into the system. Specific instrumentation used to obtain data is also discussed in Chapter III. The experimental procedures used to establish the characteristics of the system and conduct sensitivity measurements of the individual sensor coils and the gradient (dual coil) hydrophone are discussed in Chapter IV. Analysis of the data and evaluation of the results are also presented in Chapter IV. Chapter V contains concluding remarks and recommendations for further work. Appendix A lists a BASIC computer language program used in data acquisition and Appendix B presents an example of the data obtained using this program.

II. THEORY

A. CONVENTIONAL GRADIENT HYDROPHONE

In many acoustic applications it is necessary to determine the direction of signal arrival as well as to detect acoustic pressure levels. Directional features are usually achieved with the use of multiple hydrophones spatially distributed in some specified orientation, e.g., a line array. The simplest of these designs is the dipole pressure gradient hydrophone.

Some pressure gradient hydrophones are designed so that the sensing part of the hydrophone oscillates in the medium under the influence of the sound pressure gradient. That is, a hydrophone is constructed for which the driving force and the hydrophone's output is proportional to the *difference* between the pressures at two different locations in an acoustic sound field. Therefore, the electrical output is proportional to the pressure gradient in the sound field. The main characteristic and advantage of a pressure gradient hydrophone is the directivity pattern obtained from such a small size hydrophone. As will be shown below, pressure gradient hydrophones have dipole, or figure-eight, directivity patterns, as indicated in Figure 2.1; hence they are bidirectional. Assuming the size of the hydrophone is

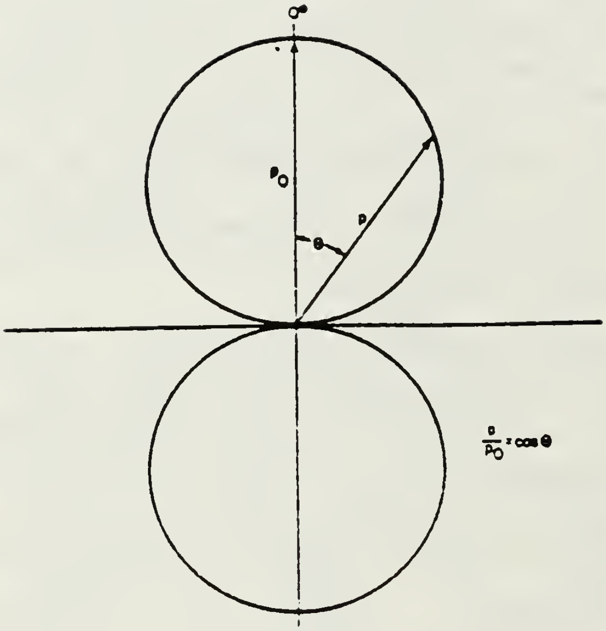

Figure 2.1 Directivity Pattern of Pressure Gradient Hydrophone

small compared to the acoustic wavelength λ, the dipole response when oriented at any angle θ relative to an incoming plane pressure wave is proportional to $\cos\theta$.

Both for simplicity and since they resemble the fiber optic system under study, pressure gradient hydrophones formed by combining two small, closely spaced, individual, pressure hydrophones will be discussed. The performance of this hydrophone pair (or doublet) is easily calculated, and the behavior thus derived applies also to pressure gradient hydrophones of more complicated construction as long as the assumptions of compactness made in the derivation are not violated.

As an introduction to the theory of this type of hydrophone, consider two small pressure hydrophones placed in a standing acoustic wave field, $P(x,t)$, separated by a distance $d \ll \lambda$ as shown in Figure 2.2. The hydrophones are placed so that a null in the standing wave pattern occurs halfway between the two hydrophones. The electrical outputs of the two are connected 180 degrees out-of-phase with each other to obtain a dipole. The dimensions of the two hydrophones are typically much less than a wavelength, therefore the acoustic field is assumed to be negligibly disturbed.

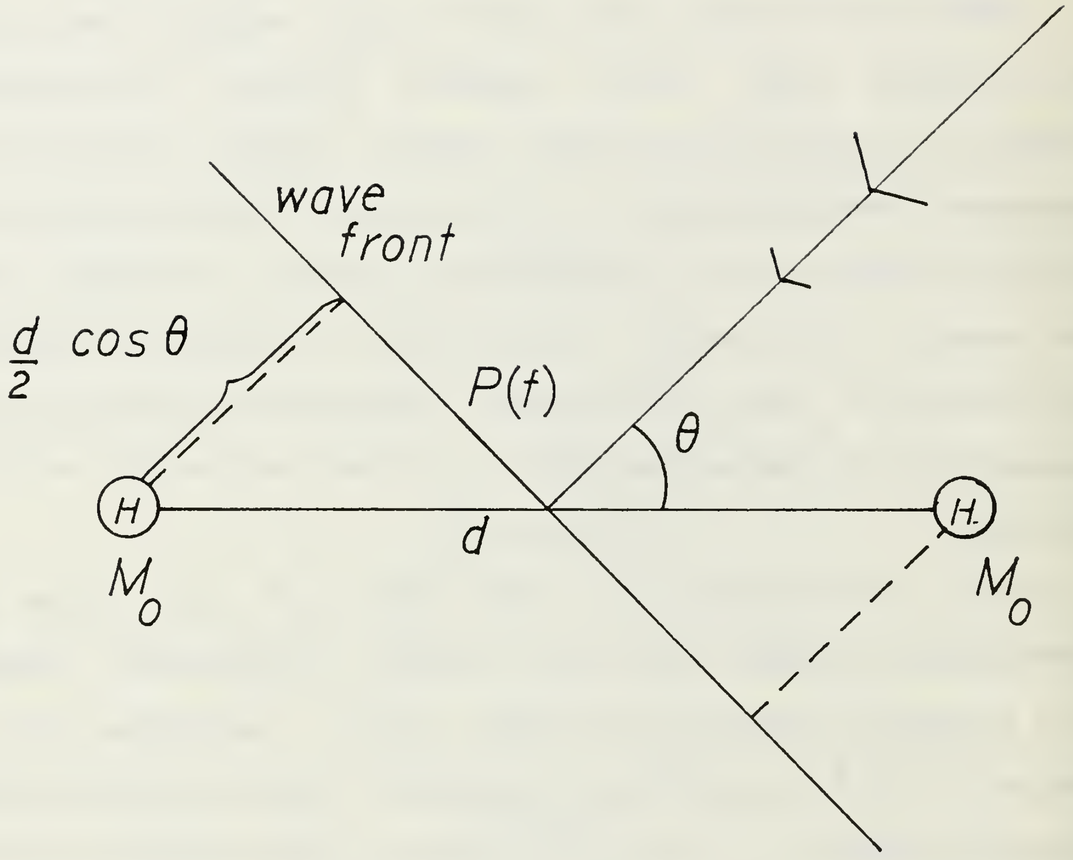

θ — angle of incidence

d — spacing between hydrophones

M_0 — individual hydrophone free field voltage sensitivity

Figure 2.2 Geometry Used in Deriving Sensing Characteristics of Acoustic Dipole (Pressure Gradient)

Consider the plane sinusoidal wave shown in Figure 2.3. The instantaneous acoustic pressure, $P(x,t)$ is given by:

$$P(x,t) = P_o \sin[kx] e^{j\omega t} \tag{2.1}$$

where P_o is the peak acoustic pressure, k is the propagation wave number $k = 2\pi/\lambda$, and x is the distance of one of the hydrophones from absolute minimum pressure (i.e. the standing wave pressure node). Assuming the argument of the sine function is small, the first order (linear) approximation (i.e., $\sin y = y$) of the pressure amplitude at x is given by:

$$P(x,t) = P_o kx\, e^{j\omega t} \tag{2.2}$$

If one sensor is at $x = -d/2$ and the other at $x = +d/2$ as shown in Figure 2.3, then the amplitude of the pressure difference to be measured may be expressed as:

$$\Delta P = P_{+d/2} - P_{-d/2} \tag{2.3}$$

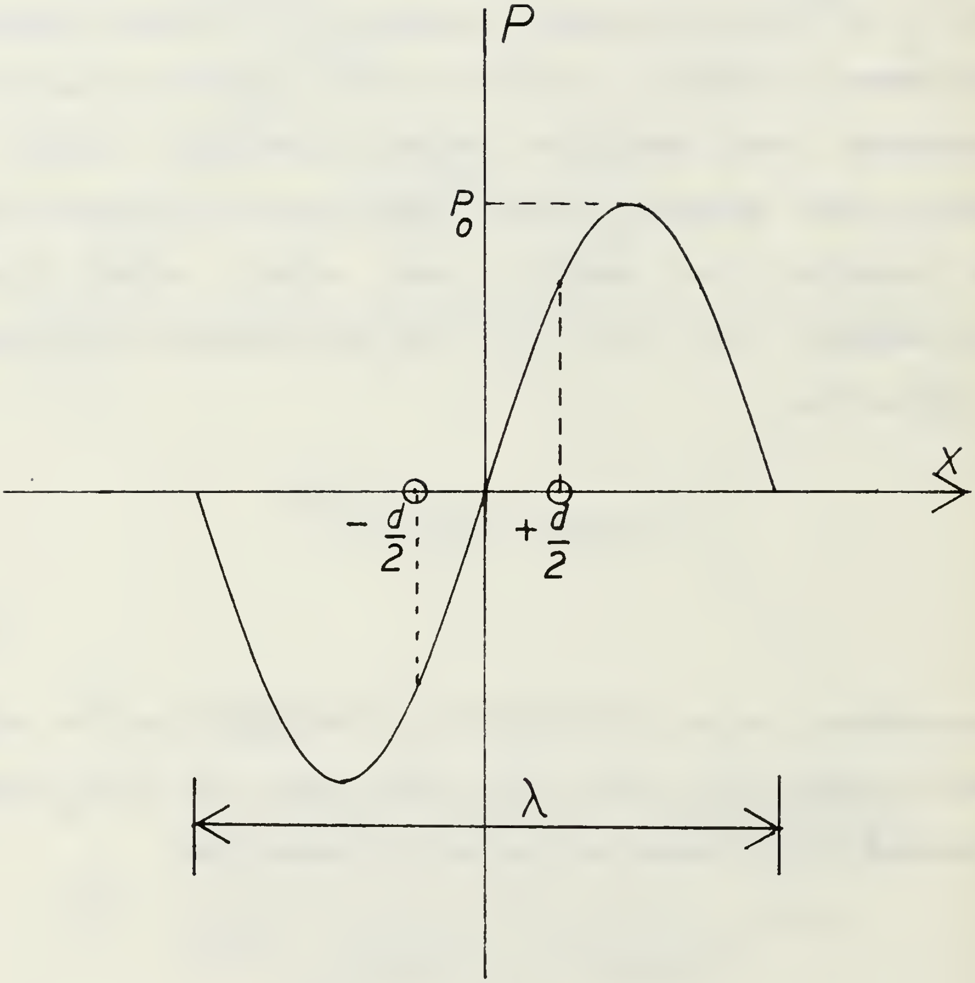

Figure 2.3 Pressure Distribution as Function of Distance from Null Pressure Point

This may be written as:

$$\Delta P = P_o k[d/2 - (-d/2)] \tag{2.4}$$

Or:

$$\Delta P = P_o kd \tag{2.5}$$

For the more general one dimensional case of any point along a standing wave, consider a standing wave in a tube of water as shown in Figure 2.4. The instantaneous acoustic pressure P(x,t) is given by:

$$P(x,t) = P_o \sin(kx)e^{j\omega t} \tag{2.6}$$

where x has been chosen to be zero at the air-water boundary.

If we expand equation (2.6) into a Taylor's series about x = h, where h is the distance from the air-water boundary, the following equation results:

$$P(x,t) = P(h,t) + \left(\frac{\partial P(h,t)}{\partial x}\right)(x - h) + \left(\frac{\partial^2 P(h,t)}{\partial x^2}\right)\frac{(x - h)^2}{2} + . . . \tag{2.7}$$

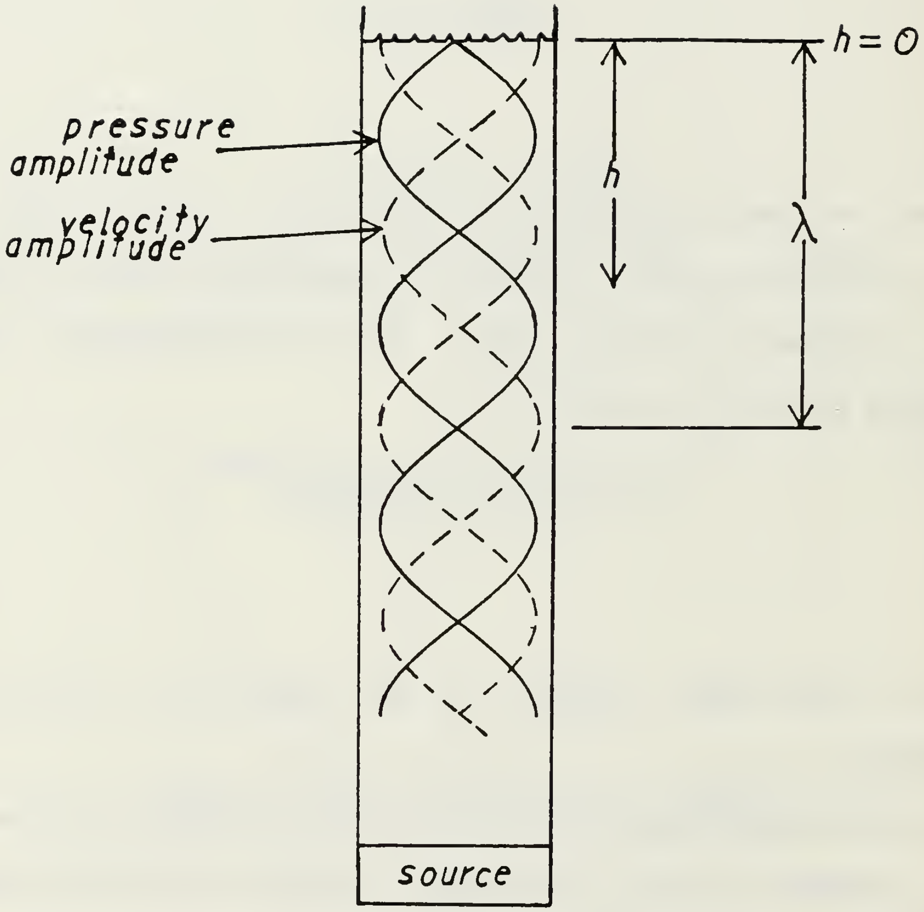

Figure 2.4 Pressure and Velocity Distribution in a Standing Wave Tube.

where the first term and all their partial derivatives are evaluated at x = h. Time t is held constant.

The first partial derivative (pressure gradient) is:

$$\partial P/\partial x = P_o k\cos(kx)e^{j\omega t} \tag{2.8}$$

The second partial derivative is:

$$\partial^2 P/\partial x^2 = -P_o k^2 \sin(kx)e^{j\omega t} \tag{2.9}$$

The pressure difference between two points axially displaced from one another by distance Δx where $\Delta x = x - h$ is:

$$\Delta P = P(x,t) - P(h,t) \tag{2.10}$$

or

$$\Delta P = (\partial P/\partial x)\Delta x + (\partial^2 P/\partial x^2)(\Delta x)^2/2 + \ldots \tag{2.11}$$

If Δx is small compared to the wavelength of the standing wave all terms above second order may be neglected and therefore the series may be truncated after the second order term.

If h and Δx are selected so that a pressure node is located at $\Delta x/2$, then the difference in pressure ΔP reduces to equation (2.5) with $\Delta x = d$, in the linear approximation. The first correction, ϵ, to the linear approximation, in the vicinity of a pressure node, becomes:

$$\epsilon = -[(k\Delta x)/2]\tan(kh) \tag{2.12}$$

A maximum in the pressure difference will occur when each sensor is equally distant from the pressure node and conversely a minimum in the pressure difference will occur when each sensor is equally distant from a pressure maximum (antinode).

A pressure gradient hydrophone is sometimes called a velocity hydrophone, the implication being that it responds to the particle velocity in the acoustic medium. This is somewhat misleading since the velocity of the hydrophone surface is normally much smaller than the particle velocity of the incident acoustic wave. But even though the hydrophone is not a direct detector of particle velocity, its response, being proportional to pressure gradient, is also proportional to particle velocity of the incident acoustic wave as shown in the one dimensional linearized Euler equation:

$$-\partial p/\partial x = j\omega\rho u \tag{2.13}$$

where ω is the angular frequency of the acoustic wave, ρ the mass density of the medium, and u is the Eulerian particle velocity of the free-field acoustic signal.

B. CALIBRATION OF GRADIENT HYDROPHONES

Pressure gradient hydrophones may be, and usually are, calibrated in terms of pressure rather than velocity (pressure gradient is never used as a reference). Since the relationship between pressure and velocity depends on the wave and boundary conditions, these conditions must be known, be standard, or fit the definition of sensitivity. Therefore the sensitivity of pressure gradient hydrophones usually is given in terms of volts/micropascals (V/μPa) specified at a particular frequency.

Plane progressive waves are specified in the definition of free-field voltage sensitivity, and the relationship between the pressure p and velocity u in such waves is given by the wave or characteristic impedance p/u = ρc. Thus, the sensitivity of a pressure gradient hydrophone expressed in terms of pressure differs from the sensitivity expressed in terms of velocity by the constant factor ρc, where ρ is the density of the medium and c is the speed of sound.

The standard procedure for pressure gradient hydrophone calibration is by direct comparison with a standard pressure hydrophone only if essentially plane waves impinge on both hydrophones. Since waves in a free field never are perfectly plane or if a spherically diverging wave from a point source is used, a correction factor, $10\log[1+\lambda^2/(2\pi r)^2]$, where r is the distance from the source, must be subtracted from the measured sensitivity [Ref. 7]. This correction factor decreases as r increases.

Because of the difficulties in obtaining free-field conditions particularly at low frequencies, a standing-wave tube like that shown in Figure 2.4 was employed for the laboratory investigations described in this report. Since a water-air boundary is a near zero impedance boundary, essentially complete reflection will take place at the top of the tube. A standing-wave system then can be established and the following relations hold in the ideal case (i.e. $SWR=\infty$):

$$p = p_o \sin kh, \tag{2.14}$$

$$u = (p_o/\rho c)\cos kh, \tag{2.15}$$

$$p/u = \rho c \tan kh. \tag{2.16}$$

If the pressure is measured at a point a distance h from the water-air surface, equations (2.14) and (2.15) can be used to compute the pressure and velocity at any other point. As stated earlier the hydrophones are assumed to have a negligible effect on the standing wave pattern. If the tube is operated below cutoff for non-axial modes, then the pressure variations normal to the tube axis can be neglected. A detailed discussion of the calibrator used is given in Chapter III section D7.

A more detailed explanation of sensitivity and calibration procedures can be found in Bobber [Ref 7]. In this experiment sensitivities of single coil fiber optic acoustic hydrophones are defined in terms of μradians/μPa. Sensitivities of gradient (dual coil) hydrophones are defined in terms of optical phase shifts induced by acoustic pressures and are expressed in μradians/μPa/cm. The procedures to obtain fiber optic hydrophone sensitivities (single and dual coil designs) are discussed in Chapter IV. A thorough presentation on fiber optic acoustic sensitivity is given by Davis, et al., [Ref. 6].

C. FIBER OPTIC ACOUSTIC SENSOR

1. Acoustically Induced Phase Modulation

Laser light conducted by optical fibers submerged in a liquid medium may be modulated (intensity or phase) by acoustic pressures. This phenomenon is exploited to make an acoustooptic sensor of underwater sound by demodulating the light using a specific detection scheme. Carome and Satyshur [Ref. 8] present in detail general fiber mode theory and the theory of phase and intensity modulation induced in optical fibers. Phase modulation occurs when the instantaneous phase angle of the lightwave in the optical fiber is varied proportionally in accordance with the instantaneous value of a modulating signal, e.g. a sinusoidally varying acoustic field.

Two major detection schemes for interferometric type sensors discussed in the references are homodyning and heterodyning [Ref. 5 and 6]. Homodyne detection in optical interferometry implies that the reference beam has the same optical frequency as the sensing beam. On the other hand, heterodyne detection is based on the use or mixing of two or more frequencies, i.e., the frequency of the reference and sensing beams differ by $\Delta\omega$. Interferometry is used in either case to recover the acoustic signal frequency. Homodyne detection was used throughout this experiment so only it will be considered in detail.

An external pressure field applied to a fiber will cause various changes in the fibers physical characteristics, such as changes of the core radius and length, and changes in the values of the optical indices of refraction of the core and cladding [Ref. 3 and 4]. For the case of pressure induced changes of index and of length, the phase shift A, produced by a change of pressure ΔP might be given as:

$$A = k_o P\ell[(\partial n/\partial P) + n/\ell(\partial \ell/\partial P)] \tag{2.17}$$

where n is the optical index of refraction of the core, k_o is the propagation constant of light in the fiber, P is the acoustic pressure, and ℓ is the length of fiber subjected to the pressure. The partial derivative $(\partial n/\partial P)$ is evaluated at constant entropy. Whatever the form of the bracketed term of equation (2.17), the phase shift amplitude A enters the analysis in identical ways so that it is possible to proceed without being concerned with its specific form.

Using a single frequency coherent laser source, the time variation of the electric field vector of the lightwave, propagating in a fiber that has been subjected to an acoustic pressure field, may be expressed as:

$$\vec{E}(t) = \vec{E}_o \exp[j(\omega_o t + A\sin(\omega_s t)] \tag{2.18}$$

where ω_o is the angular frequency of the coherent laser source, ω_s, the angular frequency of the sound field, and A is the phase shift amplitude as described above.

Phase modulation cannot be directly detected by photodetectors due to the fact that they cannot follow the instantaneous values of such high frequency variations (approximately 10^{14} Hz). Thus, in order to accomplish phase detection, an interferometric technique must be used to convert the phase modulation to intensity (amplitude) modulation prior to detection. A monochromatic laser beam is split, with part of the beam being transmitted into a reference fiber. The other beam is sent into a sensing fiber exposed to an acoustic field. Pressures exerted on the sensor fiber as a result of the sound energy density produce optical path length changes in the fiber which, in turn, cause phase modulations in the lightwave. After passing through the fibers, the two beams are then recombined. Thus the total electric field is given by:

$$\vec{E}_T = \vec{E}_1(t) + \vec{E}_2(t) \tag{2.19}$$

where

$$\vec{E}_1(t) = \vec{E}_1 \exp[j(\omega_o t + A\sin(\omega_s t)] \tag{2.20}$$

and

$$\vec{E}_2(t) = \vec{E}_2 \exp[j(\omega_o t + \phi)] \tag{2.21}$$

where ϕ is an arbitrary phase difference which will vary with temperature, the optical path difference, and other factors. $\vec{E}_1(t)$ is the electric field vector of the sensing arm and $\vec{E}_2(t)$ is the electric field vector of the reference arm. The intensity (I) of the recombined beams is proportional to the magnitude of the square of $\vec{E}_T$. Therefore, after mathematical manipulation as shown by Carome and Satyshur [Ref. 8] and neglecting terms that vary at angular frequency ω_o and $2\omega_o$, since as stated earlier they are undetectable by a photodetector, the following equation results:

$$
\begin{aligned}
I \propto \frac{E_1^2}{2} &+ \frac{E_2^2}{2} + \vec{E}_1 \cdot \vec{E}_2 \cos\phi J_0(A) \\
&+ 2\vec{E}_1 \cdot \vec{E}_2 \sin\phi J_1(A) \sin\omega_s t + 2\vec{E}_1 \cdot \vec{E}_2 \cos\phi J_2(A) \cos 2\omega_s t \\
&+ 2\vec{E}_1 \cdot \vec{E}_2 \sin\phi J_3(A) \sin 3\omega_s t + \ldots
\end{aligned}
\tag{2.22}
$$

where $\vec{E}_1 \cdot \vec{E}_2$ makes explicit the fact that the polarization directions may not be the same. The first three terms are considered the DC terms and all other terms of the series are the AC terms. Thus the resulting intensity function consists of a series of harmonics of the acoustic frequencies where the amplitude of each successive harmonic is a function of the acoustic pressure, and varies as the Bessel function of corresponding order.

If both of the beams are phase modulated by the acoustic pressure as in the case of the pressure gradient hydrophone, with phase shifts of A_1 and A_2, respectively, the final expression for the intensity is identical to equation (2.22), except that for A, the quantity $\Delta A = A_1 - A_2$ must be substituted.

The recombined lightwave with its varying intensity is then projected onto the surface of a photodetector. There results in the photodetector current a signal which is related to the acoustically induced phase shift. The photodetector current has components of the following form:

$$\begin{aligned} i(t) = {} & i_0 \cos\phi * \{J_0(k_0 x) + 2\sum_{n=1}^{\infty} J_{2n}(k_0 x)\cos[2n(\omega_s t)]\} \\ & - i_0 \sin\phi * \{2\sum_{n=0}^{\infty} J_{2n+1}(k_0 x)\sin[(2n+1)(\omega_s t)]\}, \end{aligned} \tag{2.23}$$

where J_n is the Bessel function of order n [Ref. 8], ϕ is the static phase difference, which will vary with temperature, path length difference, and other factors, $k_0 = 2\pi/\lambda_0$, where k_0 is the optical propagation constant in the fiber, λ_0 is the optical wavelength in the fiber, and x is the amplitude of the optical path-length change at ω_s. The J_0 term in equation (2.23) is the DC component associated with the acoustically induced signal with the remaining terms being the AC component. Only the AC terms of equation (2.23) will be considered in succeeding sections.

2. Feedback Stabilization

The purpose of homodyne detection in the fiber optic interferometer discussed above is to transform the optical output of the interferometer into an electrical signal proportional to the amplitude of the relative phase shift produced by a pressure oscillation at frequency ω_s. Homodyne signal processing suffers from phase drift due to small temperature and pressure variations. Any random change in length in one arm of the fiber interferometer with respect to the other arm appears in equation (2.23) as a change in the angle ϕ. As ϕ changes, the amplitudes of the AC components of equation (2.23) varies due to the factors $\cos\phi$ and $\sin\phi$. This unwanted change in the amplitude of the detected signal is referred to as signal fading. Consider the case in which the outputs of the two arms of the interferometer are initially in phase, ϕ is equal to zero, and when combined at the output coupler they interfere constructively. If now there is a small acoustically induced phase modulation e.g. at peak to peak amplitude 0.1 radian; referring to Figure 2.5, the photodetector current will oscillate about its maximum value at twice the acoustic frequency. If the length of one arm increases due to a thermal change, the average output intensity of the

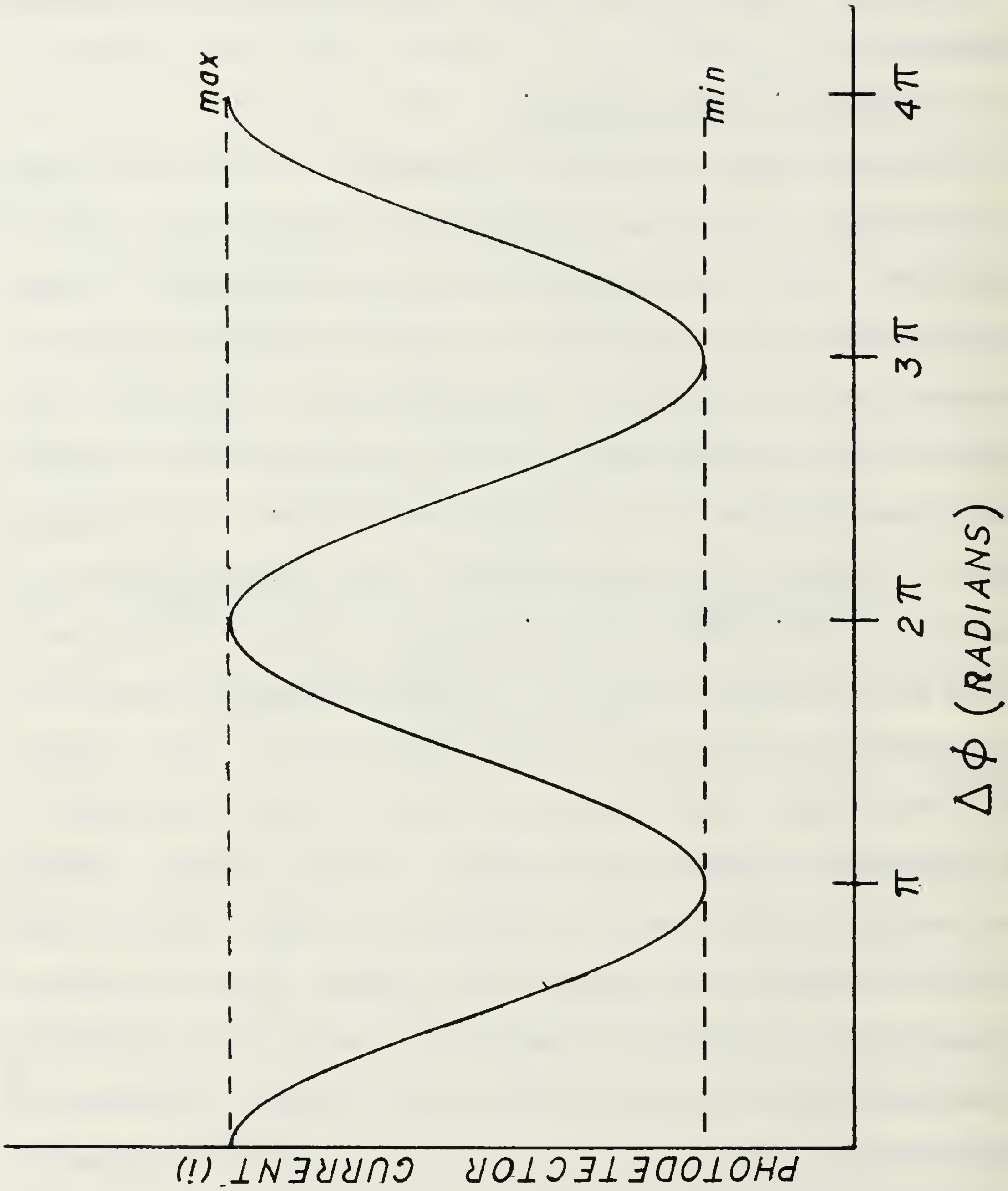

Figure 2.5 Photodetector Output Current as Function of Phase Difference between Interferometric Arms

interferometer decreases, but the acoustically induced oscillations will increase in amplitude and approach a pure sinusoidal of frequency equal to the acoustic frequency. In a practical hydrophone it is essential to maintain the interferometer continuously at its maximum sensitivity. The sensitivity to phase changes varies as the slope of the curve of Figure 2.5. The maximum sensitivity occurs for odd multiples of $\pi/2$ while essentially zero sensitivity occurs for even multiples of $\pi/2$. Therefore to maintain sensitivity a $\pi/2$ phase bias is required. This $\pi/2$ bias condition is known as quadrature.

To place the interferometer in quadrature condition for maximum sensitivity and in addition provide a means to compensate for slow drifts, a phase-locked compensator circuit is used. The circuitry required to provide and insure quadrature operation in the presence of low frequency drift is shown schematically in Figure 2.6 [Ref. 9]. The outputs of the two photodiodes are combined in a differential amplifier that provides common-mode rejection as well as amplification. This is followed by two stages of integration that provide additional amplification. These two integrator-amplifiers pass all signals from DC up to the highest frequency of interest. The output of the two stage integrator-amplifier is applied to a phase shifter located in the reference arm of the interferometer. The phase

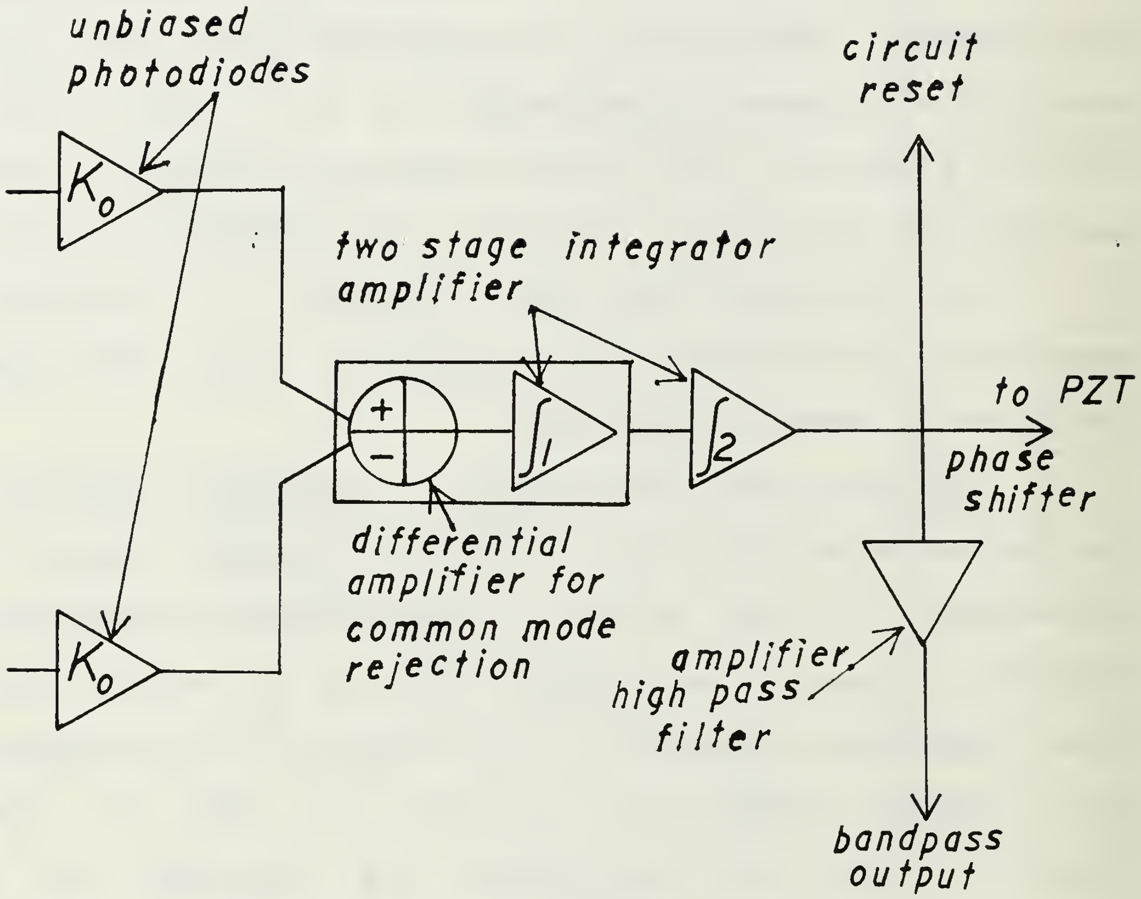
unbiased photodiodes
circuit reset
K_0
two stage integrator amplifier
$\int_1$
$\int_2$
+
−
to PZT
phase shifter
differential amplifier for common mode rejection
amplifier, high pass filter
K_0
bandpass output

Figure 2.6 Phase-Locked Loop Homodyne Detection Circuit

shifter consists of a lead zirconate-lead titanate piezoelectric (PZT) cylinder around which the fiber in the reference arm is rather tightly wound. The output of the integrator-amplifier is just equal to the voltage required to compensate for phase changes associated with the low frequency drift and that induced by the acoustic pressure signal of interest. The effect then is to produce a phase shift in the reference arm almost equal to that in the sensing arm, causing the interferometer to remain very close to perfect balance, i.e., to phase-lock the system [Ref. 10]. If the phase were exactly locked there would be no output signal from the interferometer. However, there must be an error signal or resulting phase modulation at the photodetectors in order to have a feedback signal and this is effectively 1/G times the modulation that would exist without the feedback, where G is the overall gain of the feedback circuit. If the system is initially at a bias (operating or quiescent) point away from quadrature, the effective gain will not be at its maximum value and the system will tend to drift toward its maximum gain point and therefore toward quadrature. The output signal of the feedback system represents the correction signal required to keep the phase difference between the interferometer at $\pi/2$ radians. It contains drift noise and signal information.

The signal out of the compensating circuit is also fed through a high-pass filter that has its low frequency limit set at the lowest frequency of interest but above the frequency of thermal drift etc. Therefore, the resulting output is a band of frequencies corresponding to the frequency range of interest. This constitutes the output of the interferometric sensor.

Operational amplifiers (OPAMPS) are used in the feedback circuit and complementary metal oxide semiconductor (CMOS) components in the reset circuit. The levels of voltage that can be applied by these circuits to the phase shifter are the order of ± 10 volts. On the other hand, the range that the piezoelectric phase shifter can accommodate is hundreds of volts. Furthermore, in many cases the amplitude of the phase drift resulting from temperature or pressure changes is much larger than the phase shift that would be generated by applying ± 10 volts to the phase shifter. Thus, the circuitry keeps track of how much voltage has been applied to the phase shifter and if the limit of the circuit begins to be reached it automatically and rapidly resets the circuit back to its mid range from which point it restarts the compensation process. This is the purpose of the reset circuit indicated in Figure 2.6. The phase change associated with a large amplitude slow drift is compensated by a number of saw toothed-like small amplitude phase changes. Care must be taken in the alignment of the compensation circuit to minimize noise, introduced during the reset process.

III. EXPERIMENTAL APPARATUS

A. INTERFEROMETER DESIGN AND CONSTRUCTION

Figure 3.1 shows a schematic diagram of the experimental interferometric system utilized in this study. The interferometer is modular in construction. As each module was completed proper operation was verified. A brief description of the overall construction of the interferometer is first presented; this is followed by a detailed description of each individual part.

The system is comprised of an all-fiber Mach-Zehnder interferometer. A Laser Diode Labs solid state laser was pigtailed[1] to high numerical aperture single-mode (830 nm) Corning fiber. The laser, with the pigtailed fiber, was spliced (see section on fiber preparation and splicing) to approximately half a meter of ITT single-mode fiber. The free end of the ITT fiber was then spliced to an ITT 2 X 2 all-fiber 3dB coupler. Initial attempts were made to splice the pigtailed Corning fiber directly to the coupler fiber but with limited success. Differences between melting temperatures of the Corning fiber and coupler fiber resulted

---

[1] Pigtailing of fiber to laser accomplished by laser manufacturer

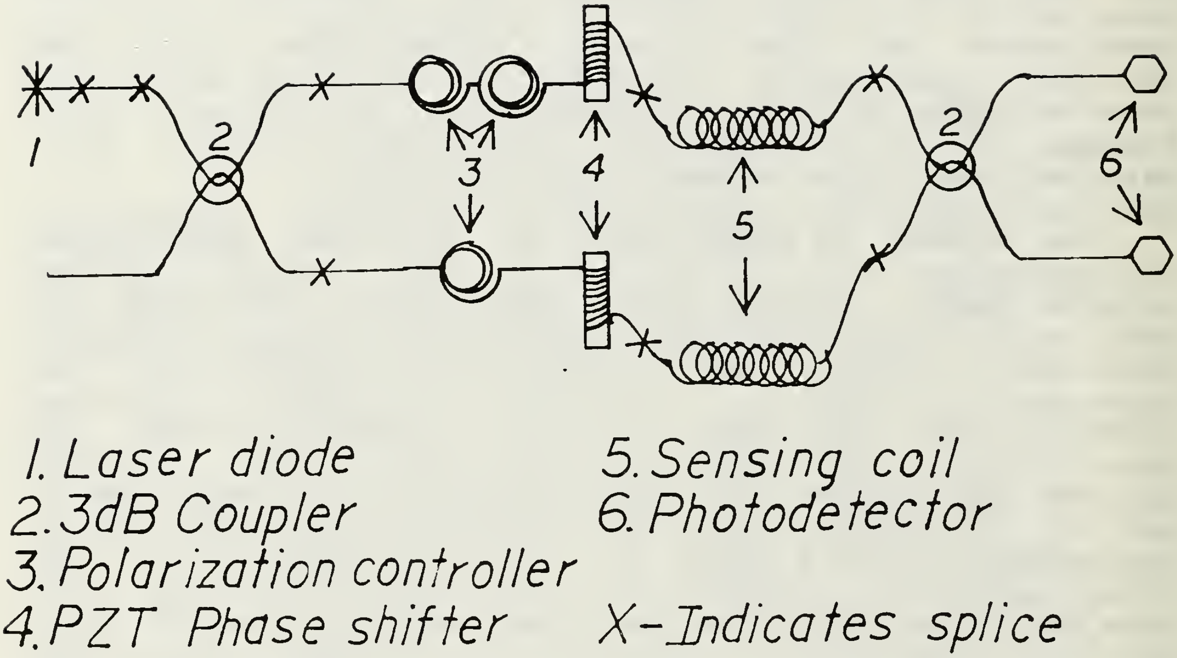

Figure 3.1 Schematic of Experimental Interferometric System.

in low strength, high loss splices. For this reason the ITT T-1601 fiber had to be used as an intermediate link between the Corning fiber and ITT coupler fiber.

The couplers themselves are all fiber counterparts of bulk optical beam splitters and equally split the light at the input end of the interferometer. Half the light is coupled to one arm and the remaining light into the other arm.

Two single-mode optical fibers with approximately equal length (estimated path length difference of approximately 2 cm) form two arms of the interferometer. Both were constructed identically; therefore only the construction of one will be discussed. Eight meters, from a ten meter length of fiber, was wrapped in a single layer onto a piezoelectric (PZT) cylinder. At each end of the wrapping approximately a meter of lead was left. One lead was then spliced to fifteen meters of fiber of which approximately ten meters was coiled into a 4 cm diameter coil. The other lead coming from the fiber wrapped around the PZT is fed through mechanical polarization controllers [Ref. 11]. One end is then spliced to one of the output leads of the input coupler and the other end is spliced to one of the input leads of the output coupler to complete construction of an arm of the interferometer. The output coupler recombines the light from the two arms. Basically the interferometer is used to convert phase modulation to intensity modulation which occurs when light from the two arms is combined. The two outputs of the interferometer are detected by two photodiodes.

Figure 3.2 is a photograph of the completed interferometer. The design of the system allows for a single coil to be placed in water to act as a pressure hydrophone or for both coils to be placed in water for operation as a pressure gradient hydrophone.

B. INTERFEROMETER COMPONENTS

1. Laser Source

The optical source used in this experimental interferometric system was a single frequency infrared laser diode optimized to emit coherent light at a wavelength of 830 nanometers. Two solid state laser diodes from Laser Diode Labs were used. The first was a CW-234 laser, pigtailed by the manufacturer with a short section of high numerical aperture single mode (830 nm) Corning fiber. The second laser, a CWX-233 laser also, pigtailed with Corning fiber, replaced the first laser after an inadvertent increase in current destroyed the CW-234 laser. Power for the laser was provided by a 12 volt 18 amp-hr Gel cell battery through a voltage regulating circuit. This circuit maintained constant current to the laser diode. Figure 3.3 is a schematic of the power supply. Before using either laser in the interferometer the end of the Corning fiber was

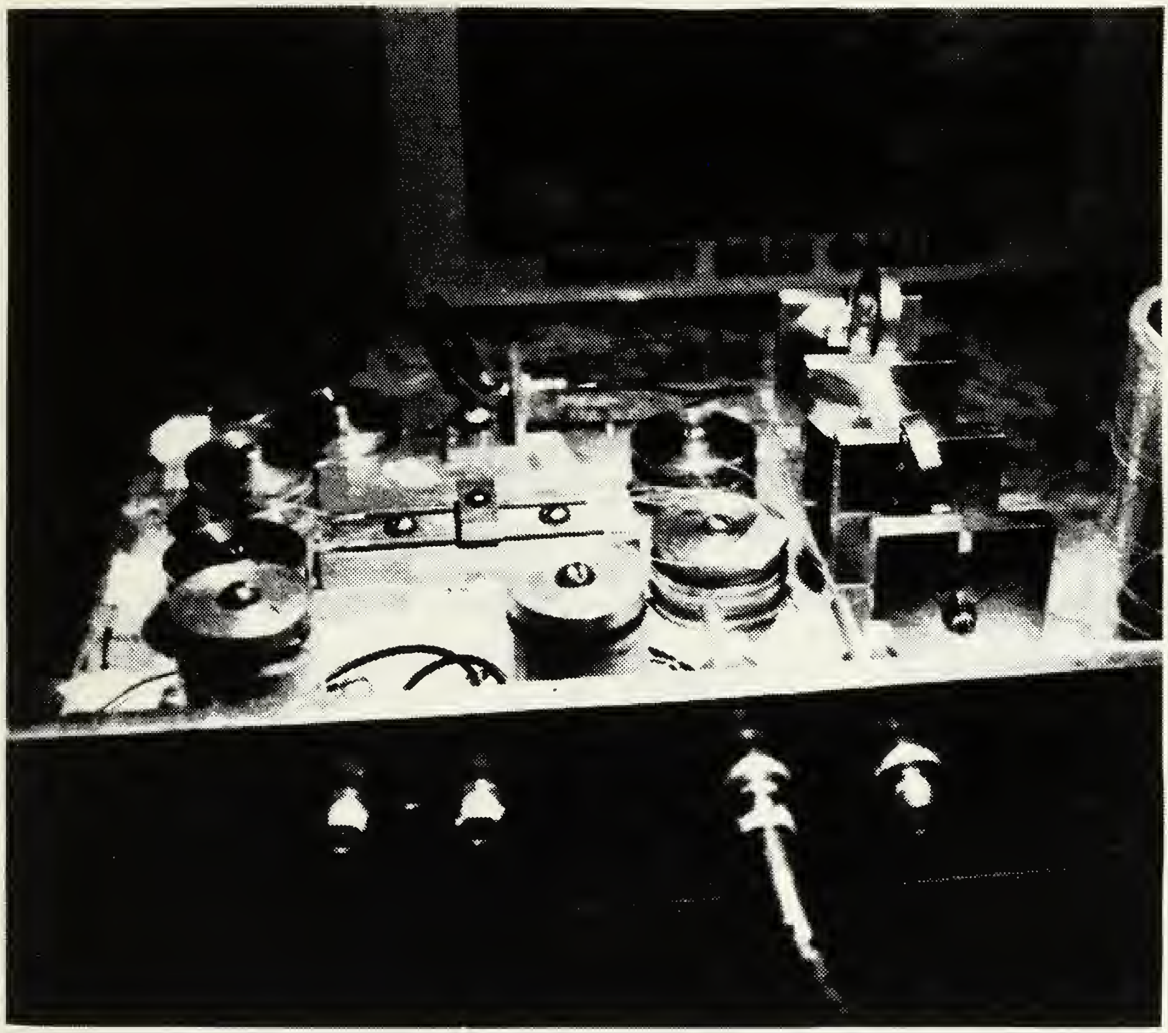

Figure 3.2 Photograph of Experimental Interferometric System

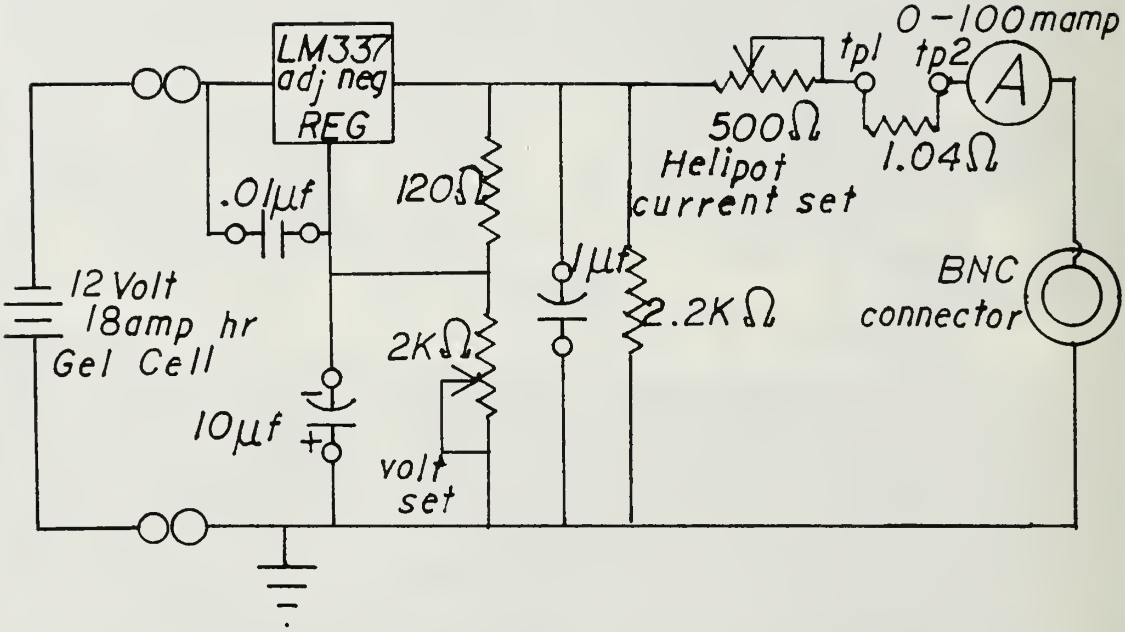

Figure 3.3 Schematic of Laser Diode Power Supply

cleaved and set up to enable a Coherent 212 optical power meter to sense the laser diode power output. As current to the laser diode was increased from 0 to approximately 53 milliamps for the CW-234 laser, and 0 to 39 milliamps for the CWX-233 laser, the power of light emitted from the laser and coupled into the fiber was read on the power meter. Figures 3.4 and 3.5 are graphs of laser power vs source current for the CW-234 and CWX-233 lasers, respectively. Extrapolating the linear region back to zero power yields a threshold current of 48.5 milliamps for the CW-234 laser and 31.3 milliamps for the CWX-233 laser. The current to the laser diode was maintained at 53 milliamps for the CW-234 laser and 35 milliamps for the CWX-233 laser during experimental testing and data acquisition.

2. Fiber Specification

The optical fiber used was ITT single-mode fiber, type T-1601[2] optimized at 0.83 microns. Specifications of fiber are as follows:

Fiber Ident: 81092U-17Bic

Preform No.: EMT-21972B

Numerical Aperture: 0.12

Core Diameter: 4.57 microns

---

[2] Optical fiber obtained from International Telephone and Telegraph, Electro Optics Products Division, Roanoake, Va 24019

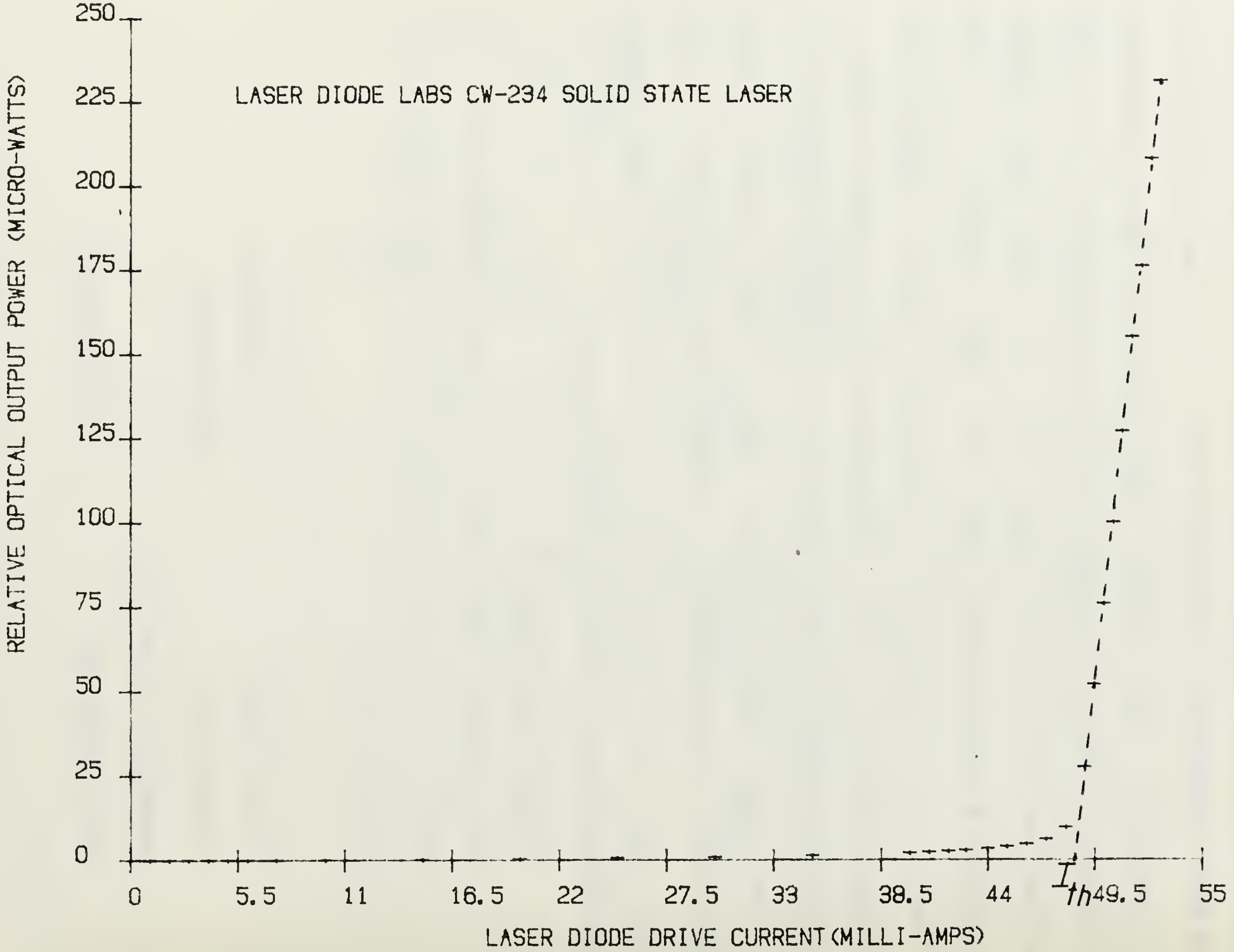

Figure 3.4 CW-234 Laser Diode Power Curve

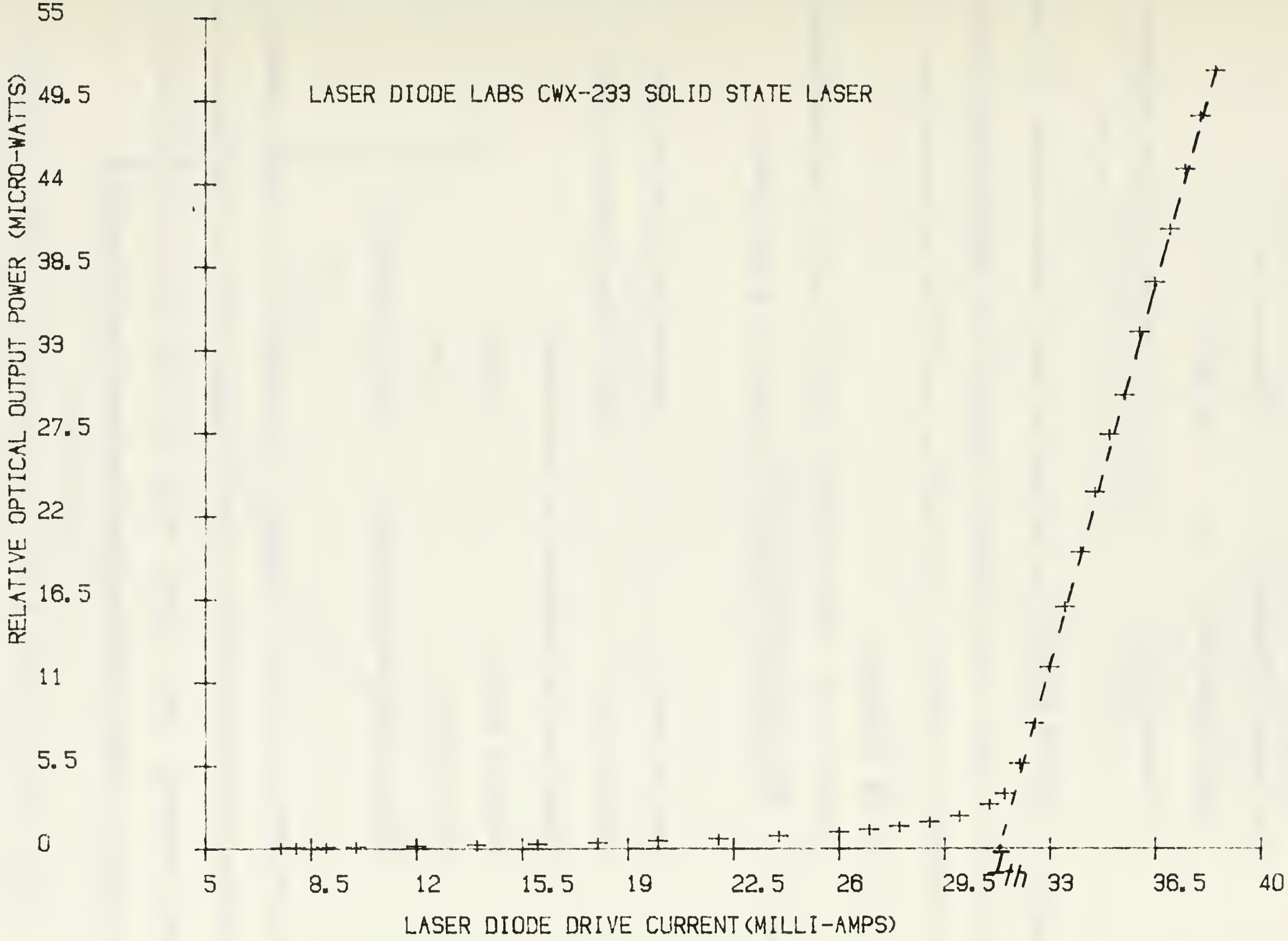

Figure 3.5 CWX-233 Laser Diode Power Curve

Outer Cladding Diameter:	75 microns
Primary Sheath:	GE 615 Silicone
Secondary Sheath:	polyester Hytrel
Total Diameter:	16 mil
Attenuation:	2.07 dB/Km at 0.83 microns

Figure 3.6 is a sketch, provided by the manufacturer of the end of the fiber, with typical dimensions, approximate index of refraction profile, and typical spectral attenuations.

3. 3 dB Coupler

The 2 X 2 single-mode couplers were also purchased from ITT. The following specifications are provided:

Serial Nos.:	JM-SM-108 & JM-SM-109
Fiber No.:	EMC 41556C/830427-401a
Fabrication Date:	6/3/83
Excess Loss:	0.1 dB
Uniformity:	0.1 dB
Operating Wavelength:	0.83 microns

The purpose of a 3 dB coupler is to split the light equally into the two arms of the interferometer or to recombine the light causing the light from the two arms to interfere in the output fibers and on the face of a photodiode.

DIMENSIONS SHOWN ARE NOMINAL VALUES

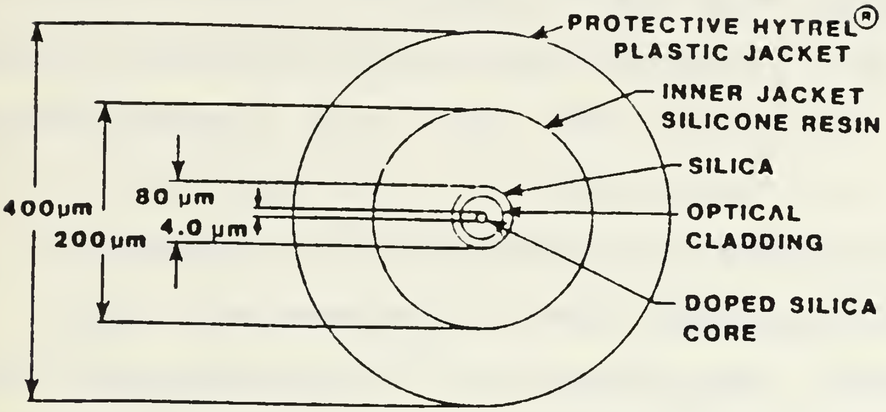
PROTECTIVE HYTREL® PLASTIC JACKET
INNER JACKET SILICONE RESIN
SILICA
OPTICAL CLADDING
DOPED SILICA CORE
400µm
200µm
80 µm
4.0 µm

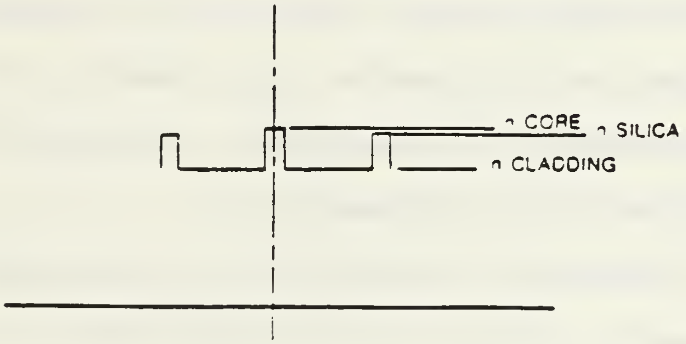

INDEX OF REFRACTION PROFILE

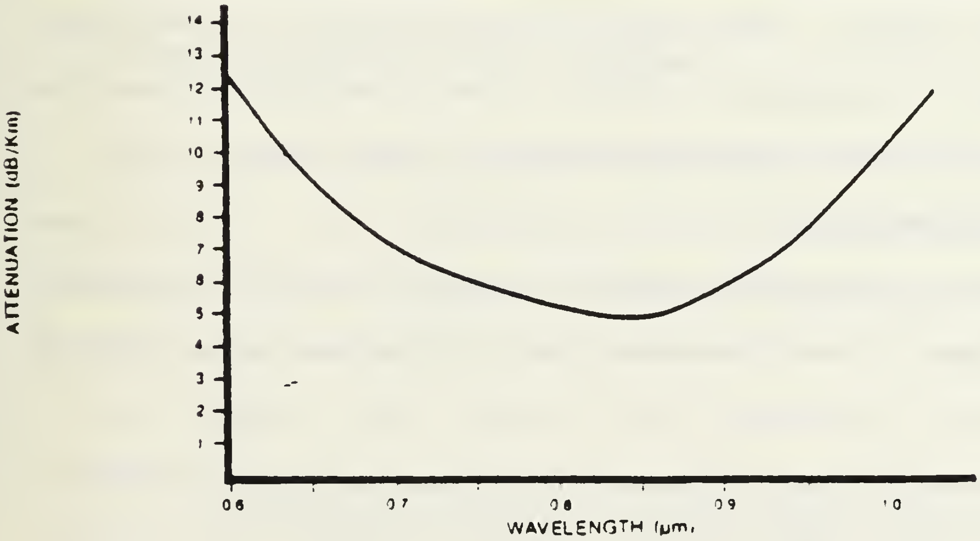

TYPICAL SPECTRAL ATTENUATION - SINGLE MODE OPTICAL FIBER

Figure 3.6 ITT Single Mode Fiber T-1601

4. Piezoelectric Phase Shifter

The phase shifter consists of a lead zirconate-lead titanate (PZT) cylinder[3] around which the fiber is tightly wrapped. The cylinders used were type Channel 5500. Each cylinder is 3.8 cm (1.5 in.) long by 3.8 cm in outer diameter with a wall thickness of 0.32 cm (0.225 in.). Two of these cylinders were incorporated into the interferometer, one in each arm. The PZT cylinders have a relatively small dynamic range but by wrapping many turns of fiber on the PZT it was possible to increase the magnitude of the phase shift. Chapter II, Section C presents the theory of operation of the PZT as a phase shifter.

5. Polarization Controller

A polarization controller, as described by Lefevre [Ref. 11], was used in this experiment. A very simple configuration is employed to control the polarization of single mode fiber. This device is equivalent to fractional wave plates of classical optics. The controller uses the stress birefringence induced by bending the fiber.

6. Photodetector

The photodetector used to detect the optical output of the fiber interferometer is a Clairex[4] type CLD-41 photodiode. They are all silicon PN planar diodes with high linearity, low dark current, and fast response. The following are the electrical characteristics as given by the manufacture:

---

[3] Piezoelectric cylinders obtained from Channel Industries, Inc., Santa Barbara, California 93105

[4] photodiodes obtained from Clairex Electronics, Mount Vernon, New York, New York 10550

Active Area: 1.3x1.3 mm
Short Circuit Current: min 6 to max 12 microamps
Open Circuit Voltage: .40 volts typical
Dark Current: 1 microamp
Junction Capacitance: 200 picofarads
Rise or Fall Time: 5 microseconds
Temperature Coefficient: +.2%/degree C typical
Peak Spectral Response: 0.91 microns

Figure 3.7 is a plot of photodiode DC voltage vs system laser optical power as measured in the laboratory using a Hewlett-Packard HP-3438A digital multimeter to measure the output voltage.

C. FIBER PREPARATION AND SPLICING

Before splicing between fibers could be accomplished, each end of the fibers had to be prepared by stripping and cleaving. Fiber stripping was accomplished in two steps. First, the outer Hytrel plastic sheath was removed by use of a razor blade. The fiber was placed on a piece of black construction paper and then a razor placed at a very small angle to it. With a slight pressure applied to the razor, the fiber was drawn out from underneath the razor. This

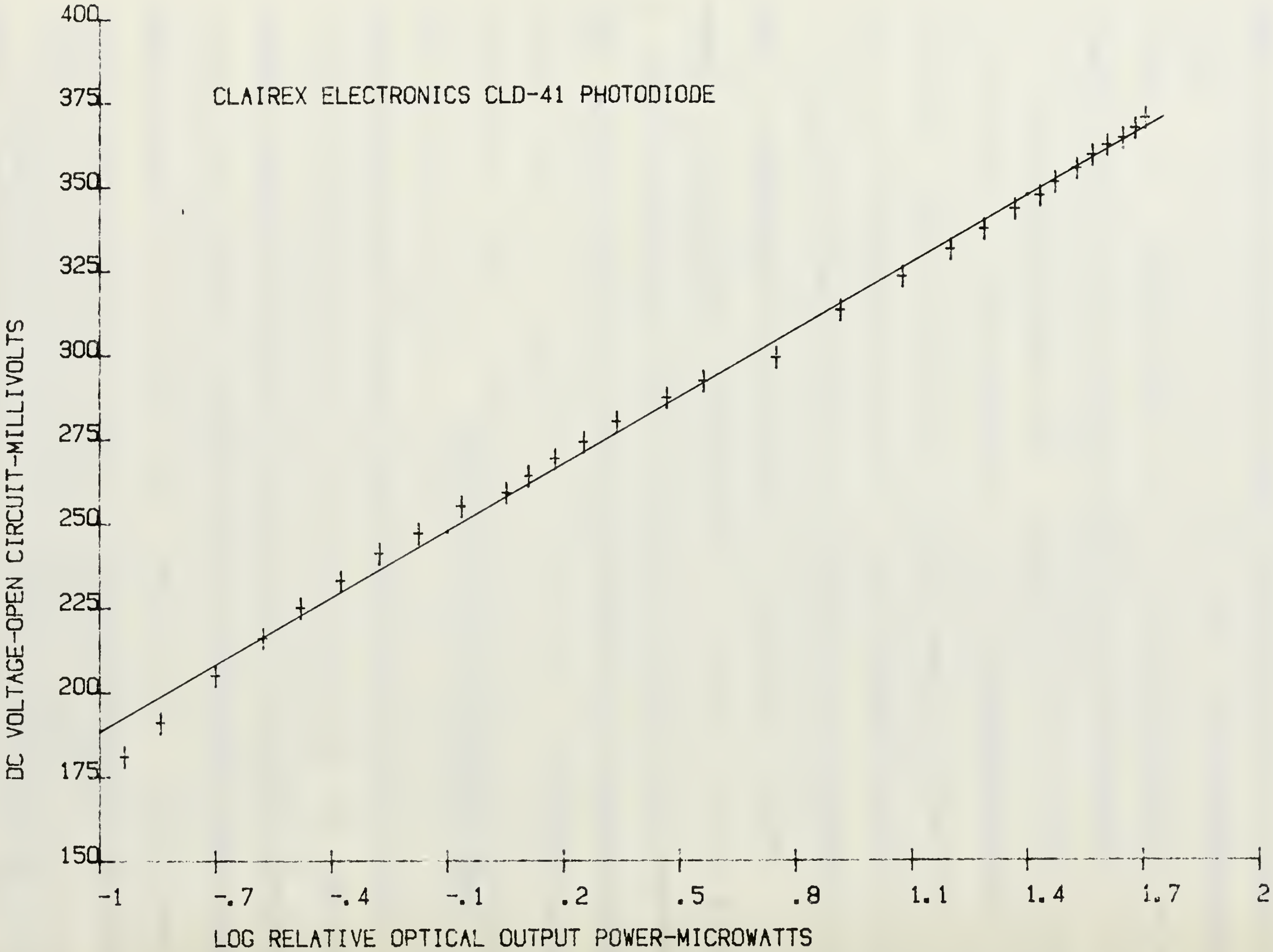

Figure 3.7 Clairex CLD-41 Relative Irradiation Curve

will carve the Hytrel jacket neatly from the fiber. By rotating the fiber and repeating this process several times, most of the outer Hytrel and inner silicone sheathing material will be removed.

The second step, that of removing any residue of inner or outer sheath that was not removed by the razor blade, is best done chemically with a solution of chromic acid. This is done by immersing the section of fiber that has been partially stripped by the razor blade in the acid for approximately two minutes. Any jacket material that remains will turn to a jelly-like consistency which is easily removed by wiping with a soft tissue. After rinsing in distilled water, the fiber is pulled between a tissue saturated with methyl alcohol. If the fiber is completely clean of the jacket a squeaking sound will be heard. At this point the fiber is bared to the silica cladding and must be handled with caution. An unscratched fiber has very high tensile strength, but will break easily if scratched and bent.

In order to insert and extract light efficiently to obtain a low loss splice, the ends must be flat and perpendicular to the longitudinal axis of the fiber. The process utilized to achieve this was cleaving. To cleave the fiber, the ends are first stripped back about two centimeters longer than needed. After preparation for cleaving, the fiber was held with slight tension and carefully touched to the cleaving blade at a point approximately 2 cm from the end of the fiber.[5] The cleaved area was then placed on a smooth, round mandrel that has a radius of approximately four centimeters. The fiber was held with thumb of one hand. Maintaining modest tension, the fiber was pulled around mandrel with other hand. When scored area reaches mandrel, a clean break will usually result. Experience showed that if the fiber broke while being scored it would have a bad end face.

To check the cleave, the fiber is inspected under a microscope. Angular breaks other than 90 degrees will not make a good low loss splice. In addition, chips and barbs at the cleaved ends will not allow satisfactory splices. Figure 3.8 shows a good cleave along with improper cleaves.

Splicing of fiber was accomplished using an electrical arc welder. The type of welder used was a Power Technology, Inc. portable fiber splicer model PFS-240. Basic splicer operations of prefusing and fusing for monomode fiber were done in accordance with the operating manual. Thumbwheel settings which controlled splicer arc amperage and the time variation of the arc current usually used are as follows:

Ramp Time	Arc Time	Arc Current
0.1 sec	0.6 sec	16 mA

---

[5] Sapphire cleaver obtained from General Fiber Optics, Caldwell, New Jersey 07006

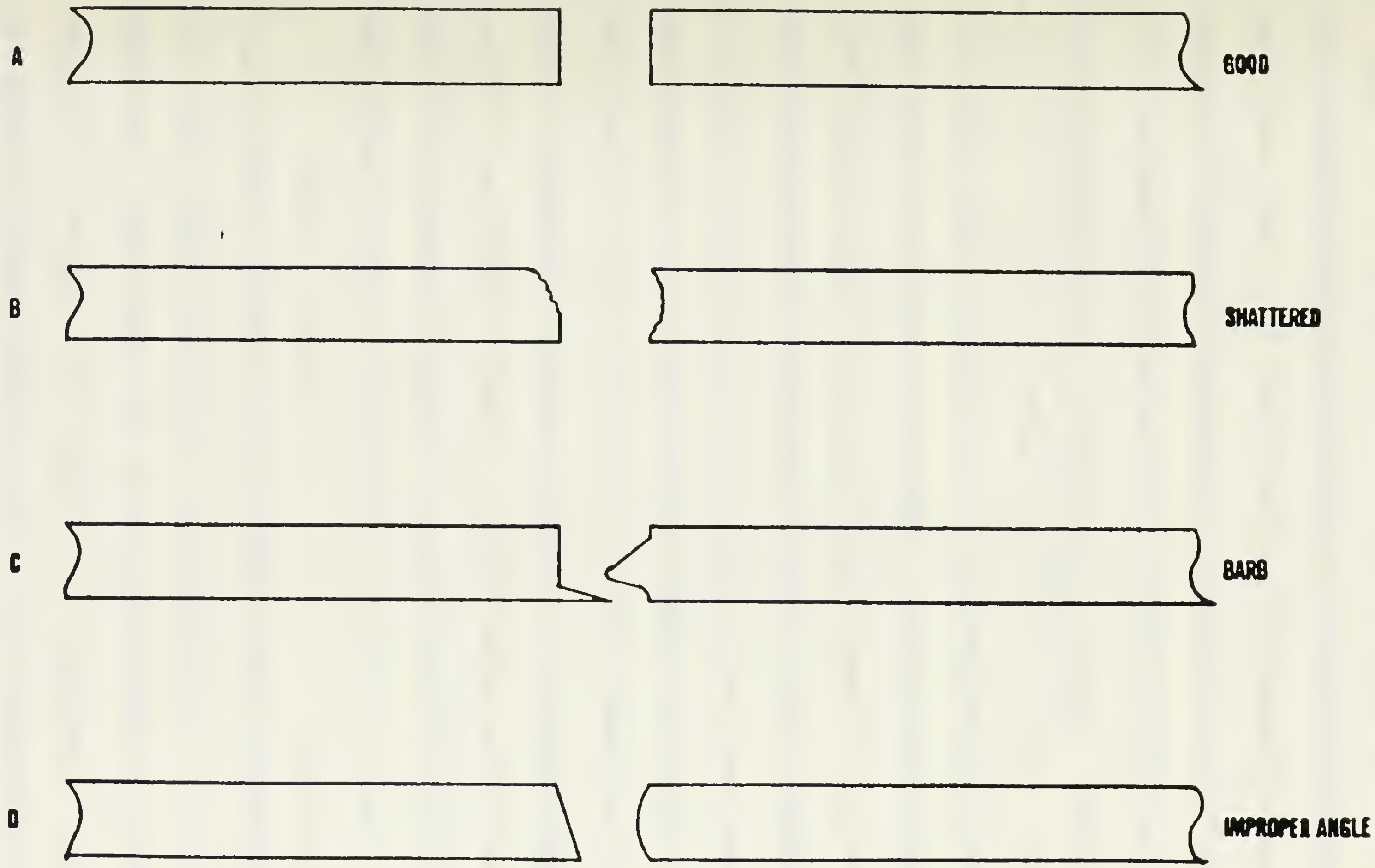

Figure 3.8 Representation of Proper and Improper Cleaves

Final alignment of cores for maximum light transmission was used to produce a low-loss splice. The micro-positioners on the splicer were adjusted to bring the prepared ends of the fiber into close alignment. Light from the laser was injected into the free end of one of the fibers, transferred across the proposed splice to the second fiber, and the output from the latter was projected onto the face of the power meter's photodiode. The micropositioners were adjusted until the power meter indicated that the transmission across the splice was maximum. At that point the fiber ends were brought together, heated by the arc welder and fused. As the joint cools, surface tension will pull the fibers into final alignment. Reports in the literature indicate that losses obtained by fusion splicing may be as low as 0.1's dB. However, in this study many hours of practice were required to obtain good (i.e. less than 3dB loss) splices. Nine splices are required in the configuration of the experimental system described above. The average loss from each splice was approximately 1dB and the total loss of the constructed interferometer was approximately 8.4dB.

Prior to projecting light from the end of the fiber onto the surface of a photodiode, the end of the fiber was prepared in the same manner as for splicing with the exception that the length of fiber that had its sheath removed was painted black. Painting was used to accomplish mode stripping. Cladding light was stripped prior to reaching the end of the fiber, thus only core light was detected by the photodiode. In splicing each additional fiber element into the system it was necessary to mode strip its output end just before the energy meter to ensure that only core light is detected, i.e. to absorb unwanted light that may reach the output end via the cladding.

D. INSTRUMENTATION AND DATA ACQUISITION

Basic block diagrams of the experimental systems used to obtain data on interferometer performance will be shown in Chapter IV as the experimental procedures are discussed. Computer data acquisition was used for portions of the data taking. The Hewlett-Packard HP-85F computer coordinates the peripherals and records and displays the data. The printer and plotter are non-essential to the system and were used to provide larger format graphics and printouts than are available with the built-in thermal printer provided with the HP-85F. The following is a brief description of each individual piece of equipment.

1. HP-85F Computer

The HP-85F is an eight bit microprocessor that utilizes BASIC computer language. The computer has as standard 16K bytes of read/write memory. 16K bytes of additional memory were added to the system giving a total of 32K bytes. The HP-85F has a 127 millimeter diagonal black and white electromagnetic CRT. A 32 character per line thermal printer/plotter is part of the unit. Programs or data may be stored on and read from magnetic tape cartridges. To interface with peripheral equipment, an I/O ROM and an interface card were added to provide HP-IB (IEEE standard 488-1975) instrumentation capabilities.

2. Arbitrary Waveform Generator HP 3314A

The Hewlett-Packard Model 3314A arbitrary waveform generator can produce three different pre-programmed waveforms; sine, square, and triangular. This instrument has a frequency range of 1 microHertz to 20 megaHertz. Output amplitude is 0 millivolts to 10 volts peak to peak into a fifty ohm load. This model is fully programable through a HP-IB connection. For this experiment sine waves of various frequencies and amplitudes were usually generated. During alignment of the locking circuit, however, a small amplitude 100 Hertz square wave was used.

3. Spectrums Analyzer HP 3582A

The Hewlett-Packard Model 3582A is a dual channel spectrum analyzer. This instrument has a frequency range of 0.02 Hertz to 25,600 Hertz. The analyzer has a 11.9 by 9.6 cm CRT that can display two simultaneous information traces, plus four lines of alphanumeric data giving measurement configuration and results. Frequency spans from 1 Hertz to 25,000 Hertz full scale allow flexibility in selecting the portion of the spectrum to be analyzed. Spans from 5 Hertz to 25,000 Hertz can be positioned anywhere within the frequency range of the instrument to provide excellent frequency resolution. The instrument's "front-end" sensitivity ranges can measure and analyze from 1 micro-volt to 31.6 volts and has a dynamic range of 70 dB.

4. Oscilloscope Tektronix 2215

The Tektronix Model 2215 oscilloscope is a dual channel, 60 MHz instrument. Its vertical system provides calibrated deflection factors from 2 millivolts to 10 volts per division. Trigger circuits enable stable triggering over the full bandwidth of the vertical system. The horizontal system provides calibrated sweep speeds from 0.5 seconds per division to 50 nanoseconds per division.

5. Digital Multimeter HP 3438A

This multimeter was utilized to obtain rms voltage readings of an LC-10 hydrophone output and transmit this via the HP-IB to the HP-85 computer.

6. Standard Hydrophone LC-10

An LC-10 hydrophone[6], Serial No. 2341 was used as the standard hydrophone for sensitivity calculations of the single coils and of the dual (gradient) coil setup. Average free field voltage sensitivity for this hydrophone is specified by the manufacture to be -209.2 dB re 1 Volt/μPa.

---

[6] Hydrophone manufacture is Celesco Ind., Canoga Park, California, 91304

This hydrophone and an USRD type F27 reversible transducer were used in another experiment [Ref. 12] to obtain a reciprocity calibration of an USRD type F33 transducer. The sensitivity for the LC-10 hydrophone obtained from the experiment was within 2 dB of manufacturer's specifications between 5 an 30 KHz.

7. Acoustic Calibrator

An acoustic system was constructed for calibrating hydrophones of various types by the comparison method. Figure 3.9 shows the calibrator in the lab, and Figure 3.10 shows the details of construction. The calibration section consists of an open-ended column of water excited by a moving-coil driver. A USRD type J11 transducer is used as the driver. The calibration chamber consists of a 6 inch inner diameter, 1/4 inch thick PVC 1120 tube (ASTM 1785), mounted on a rim around the face of the driver. Compensation for the hydrostatic pressure of the water on the face of the driven piston is provided by the airtight enclosure mounted under the driver assembly. A manometer is used to measure the equalizing pressure. A valve is opened and air is pumped into the equalizing chamber until the internal air pressure is equal to the water pressure on the upper face of the driver. This system is similar in design to the USRD type G40 shipboard calibrator used by the U.S. Navy [Ref. 13], based on article by Schloss and Strasberg [Ref. 14].

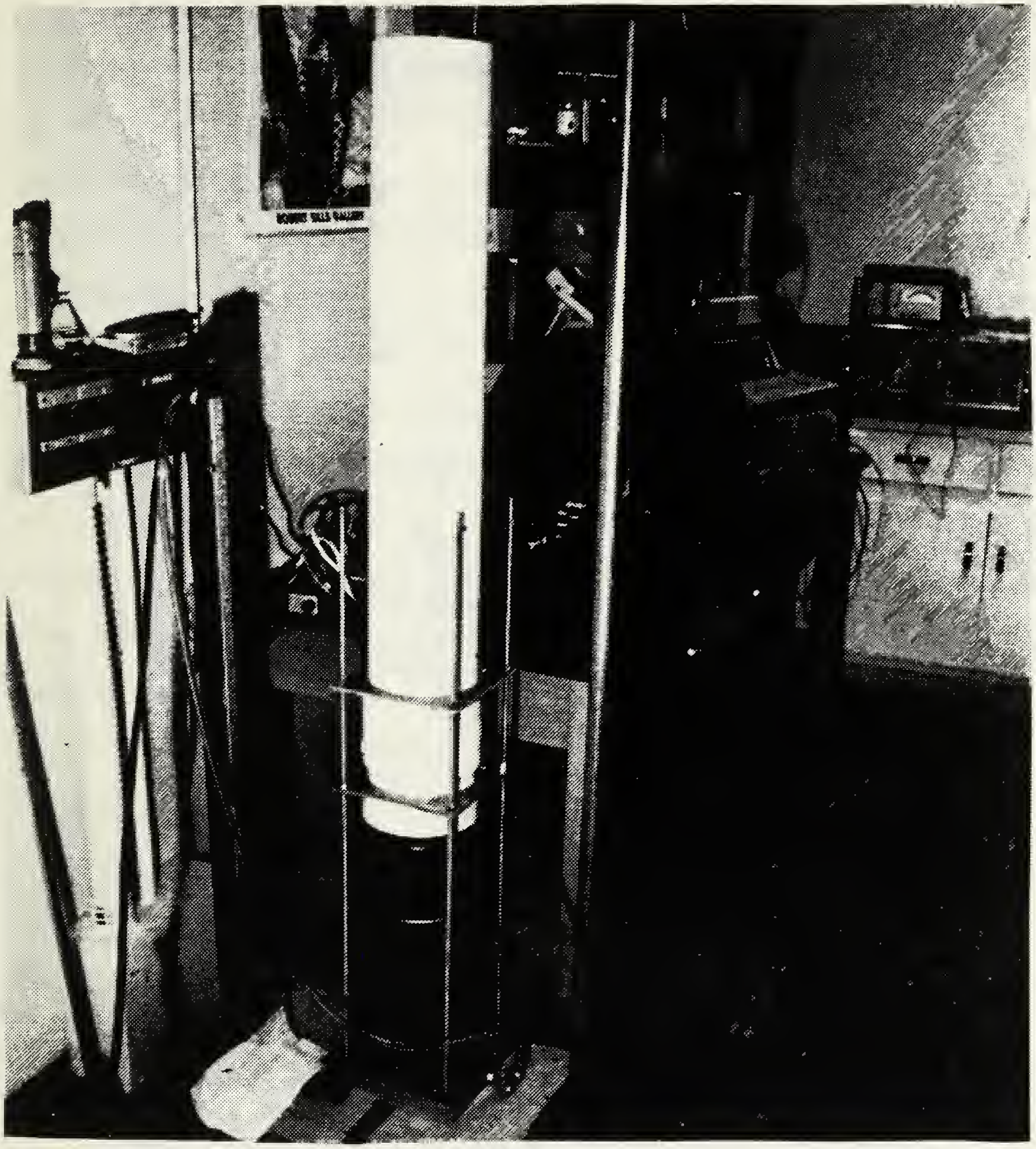

Figure 3.9 Photograph of Acoustic Calibrator

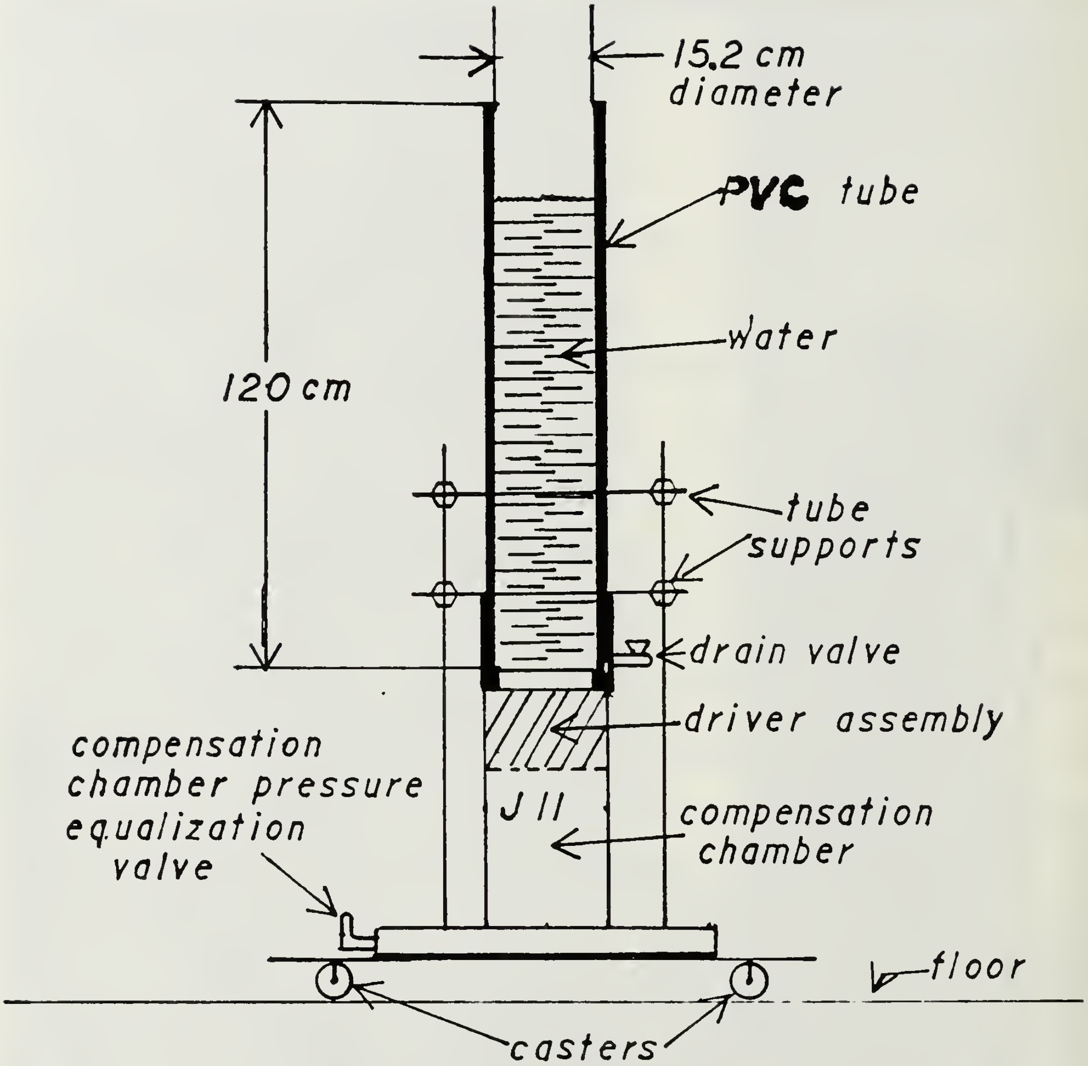

Figure 3.10 Sectional View of Acoustic Calibrator.

The compliance of the PVC tube reduced the speed of sound of the water in the calibrator to approximately 1/5 of the normal speed of sound in water. This was useful in the experiments since it reduced the wavelength λ by a factor of 5 at any given frequency and resulted in a larger gradient. Figures 3.11, 3.12, and 3.13 show the standing wave acoustic field at three resonant frequencies of the calibrator. The figures are graphical plots of LC-10 hydrophone voltage as a function of position in the calibrator. By measuring the distance of a half wavelength at the three resonant frequencies the speed of sound in the calibrator can be calculated. From the data shown in Table I an average value of 358.3 meters per second with a standard deviation of 8.6 m/sec for the speed of sound in the calibrator is calculated. The data was gathered over a period of one month.

TABLE I

Sound Speed in Calibrator

Frequency (Hz)	Half Wavelength (cm)	Speed of Sound (m/sec)
390	44.5	347.1
390	44	343.2
391	45.5	355.8
595	30	357.0
593	31	367.7
593	30.5	361.7
593	30.5	361.7
593	30.5	361.7
752	24.5	368.5
	average >>>	358.3 + 8.6

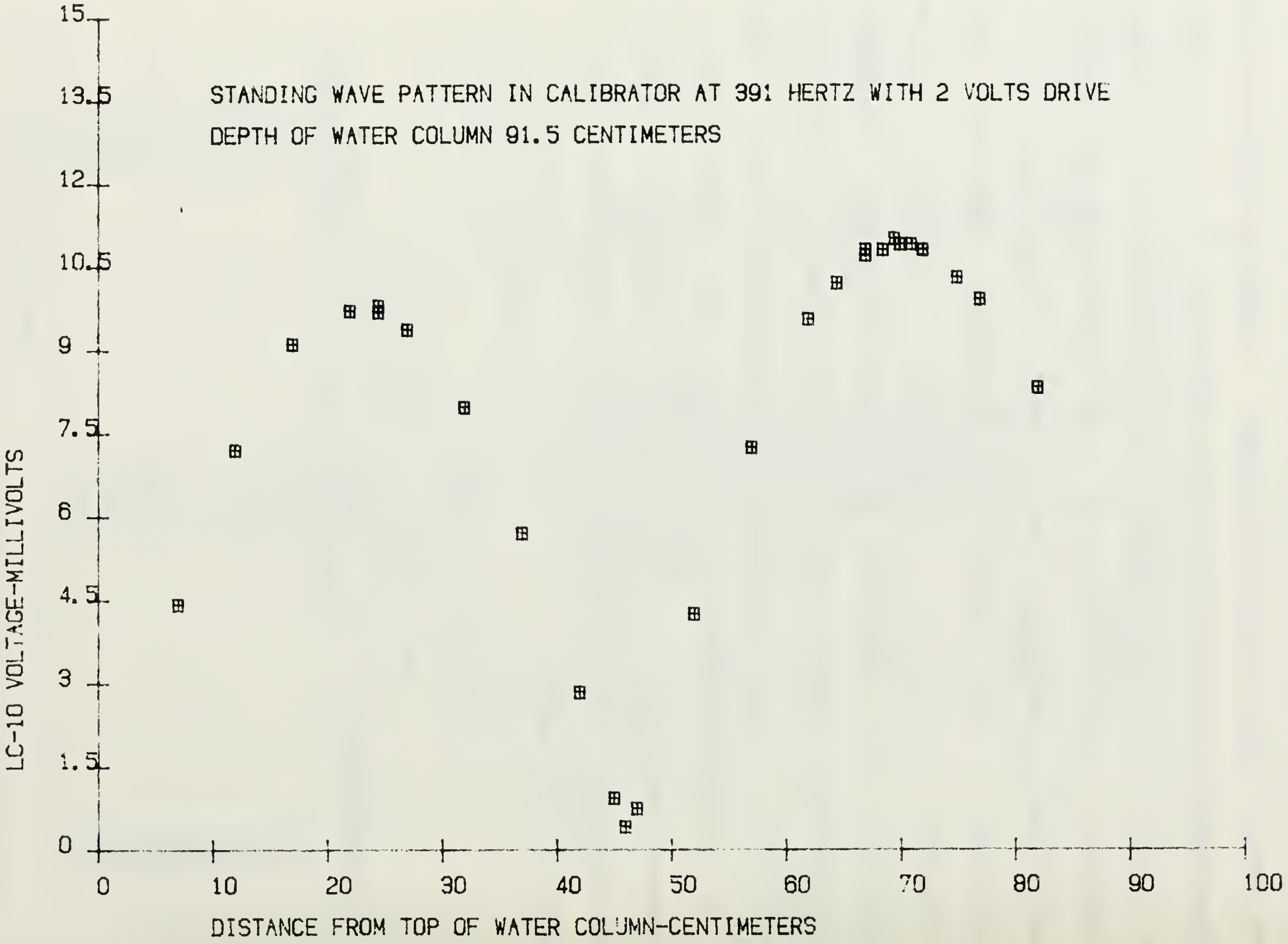

Figure 3.11 LC-10 Voltage in Calibrator at 391 Hz

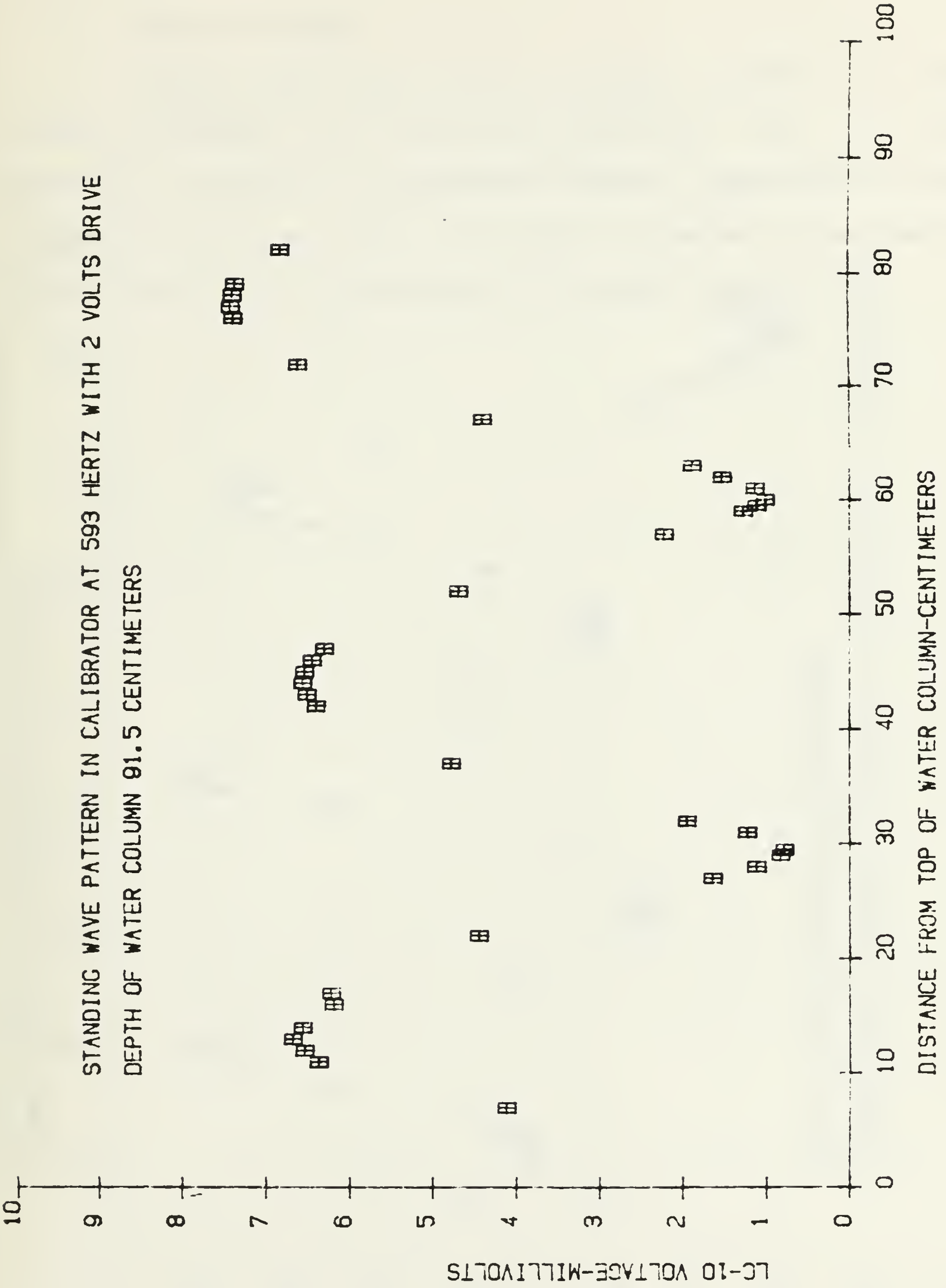

Figure 3.12 LC-10 Voltage in Calibrator at 593 Hz.

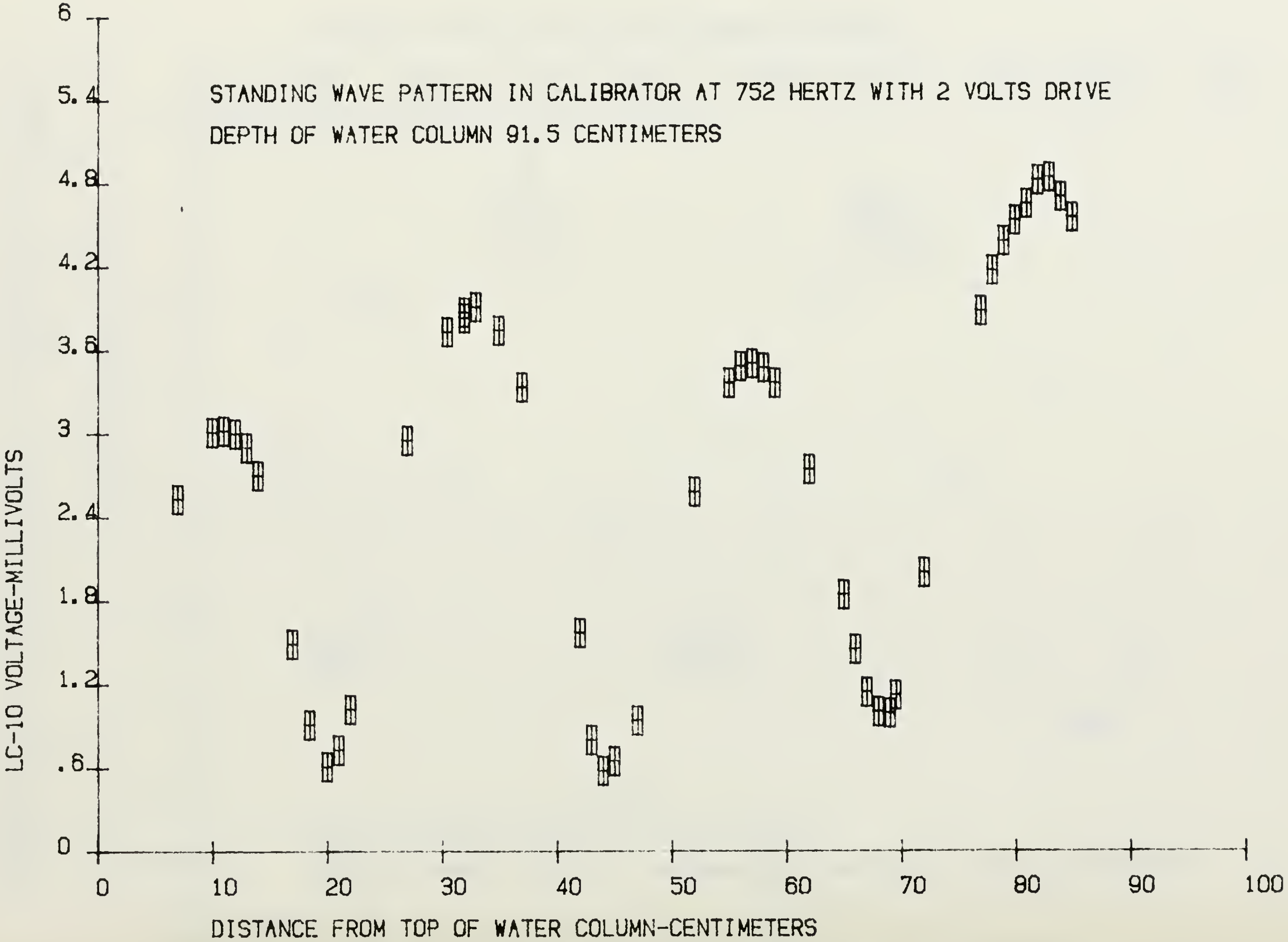

Figure 3.13 LC-10 Voltage in Calibrator at 753 Hz

8. Locking Circuit

A phase lock loop locking circuit similar to the circuit presented by Fritsch and Adamovsky [Ref. 9] and discussed in Chapter II was used to verify operation of the interferometer as a single and dual (gradient) hydrophone system. Data will be presented in the next chapter.

IV. EXPERIMENTAL PROCEDURE AND RESULTS

A. INTERFEROMETER CHARACTERISTICS

After construction of the interferometer was completed, testing was conducted to verify proper operation of the interferometer as a sensor. The initial tests consisted of detailed measurements taken to determine the amplitude of the optical phase shift as a function of the drive voltage applied to the piezoelectric cylinder in one of the arms of the interferometer. Figure 4.1 shows a block diagram of the instrumentation required for operating the system. A variable amplitude sine wave of frequency f from the function generator was applied to the PZT cylinder. A Tektronix 2215 oscilloscope and a HP 3582A spectrum analyzer were used to detect the output of one of the photodiodes.

The behavior of a Mach-Zehnder fiber interferometer was treated in detail in Chapter II. Recall that the AC portion of the photodiode current is given by the following equation:

$$\begin{aligned} i(t) = {} & i_0 \cos\phi * \left[2 \sum_{n=1}^{\infty} J_{2n}(k_0 x) \cos[2n(\omega_s t)] \right] \\ & - i_0 \sin\phi * \left[2 \sum_{n=0}^{\infty} J_{2n+1}(k_0 x) \sin[(2n+1)(\omega_s t)] \right] \end{aligned} \tag{4.1}$$

where J_n is the Bessel function of order n.

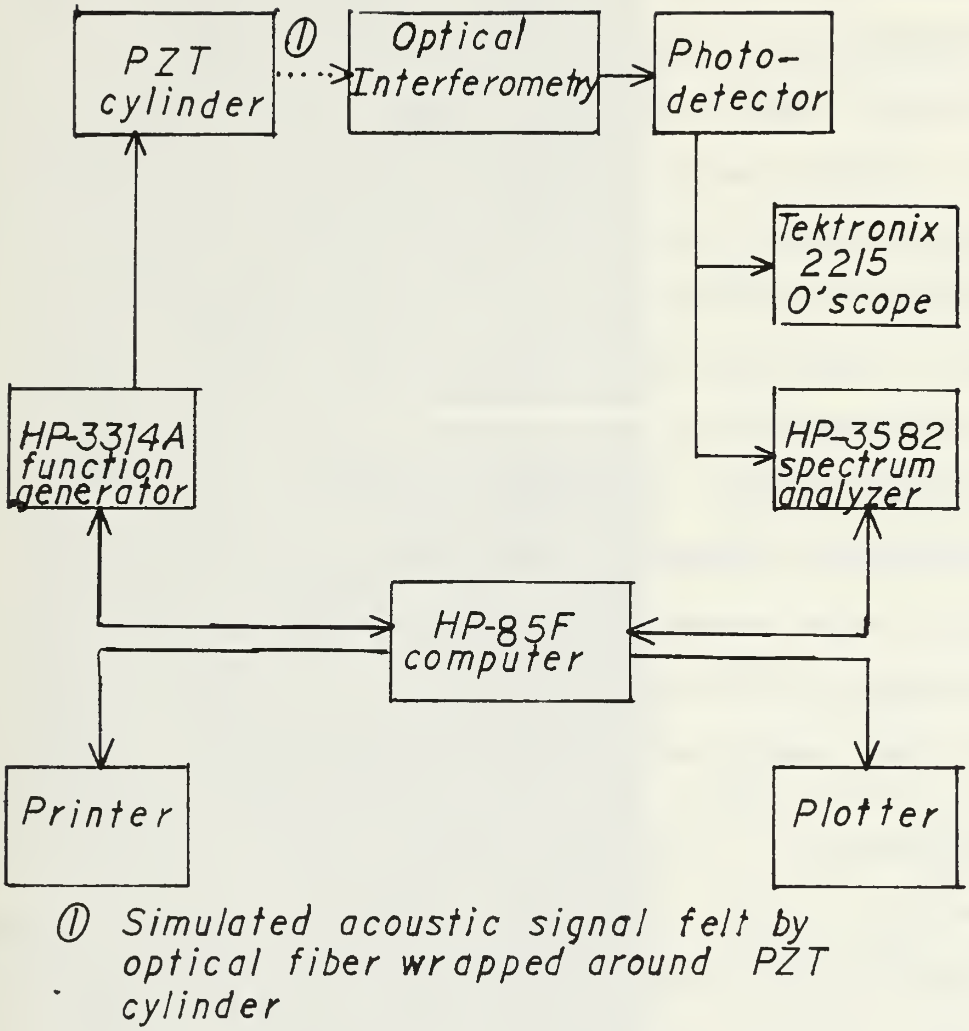
PZT cylinder
①
Optical Interferometry
Photo-detector
Tektronix 2215 O'scope
HP-3582 spectrum analyzer
HP-3314A function generator
HP-85F computer
Printer
Plotter
① Simulated acoustic signal felt by optical fiber wrapped around PZT cylinder

Figure 4.1 Block Diagram of Instrumentation Setup

From equation (4.1) it is clear that as the phase shift $k_0 x$ is increased the photodiode output becomes non-linear and harmonics of the drive signal begin to appear. This is illustrated in Figure 4.2 where oscillograms of the photodiode output signal are shown for successively higher drive signals applied to the piezoelectric cylinder. In each oscillogram the drive signal is shown in the upper trace and the corresponding photodiode output signal is shown in the lower one.

The magnitude of the optical phase shift as a function of drive voltage may be determined quantitatively by examining the frequency spectrum of the photodiode output signal. From equation (4.1) it may be seen that the amplitudes of the various n^{th} order harmonics should have nulls for phase shifts $k_0 x$ equal to the zeroes of the corresponding n^{th} order Bessel functions. This behavior is illustrated in Figure 4.3 where the photodiode voltage is plotted for the fundamental and first two harmonics vs drive voltage applied to the piezoelectric cylinder. The data were obtained with the computer data acquisition equipment discussed in chapter III. A computer program for the HP-85F computer, listed in Appendix A, was written in BASIC computer language to control the peripheral equipment. A fundamental frequency, lower and upper limits of amplitude, and an incremental value are selected. The function generator and spectrum analyzer are preset and configured to

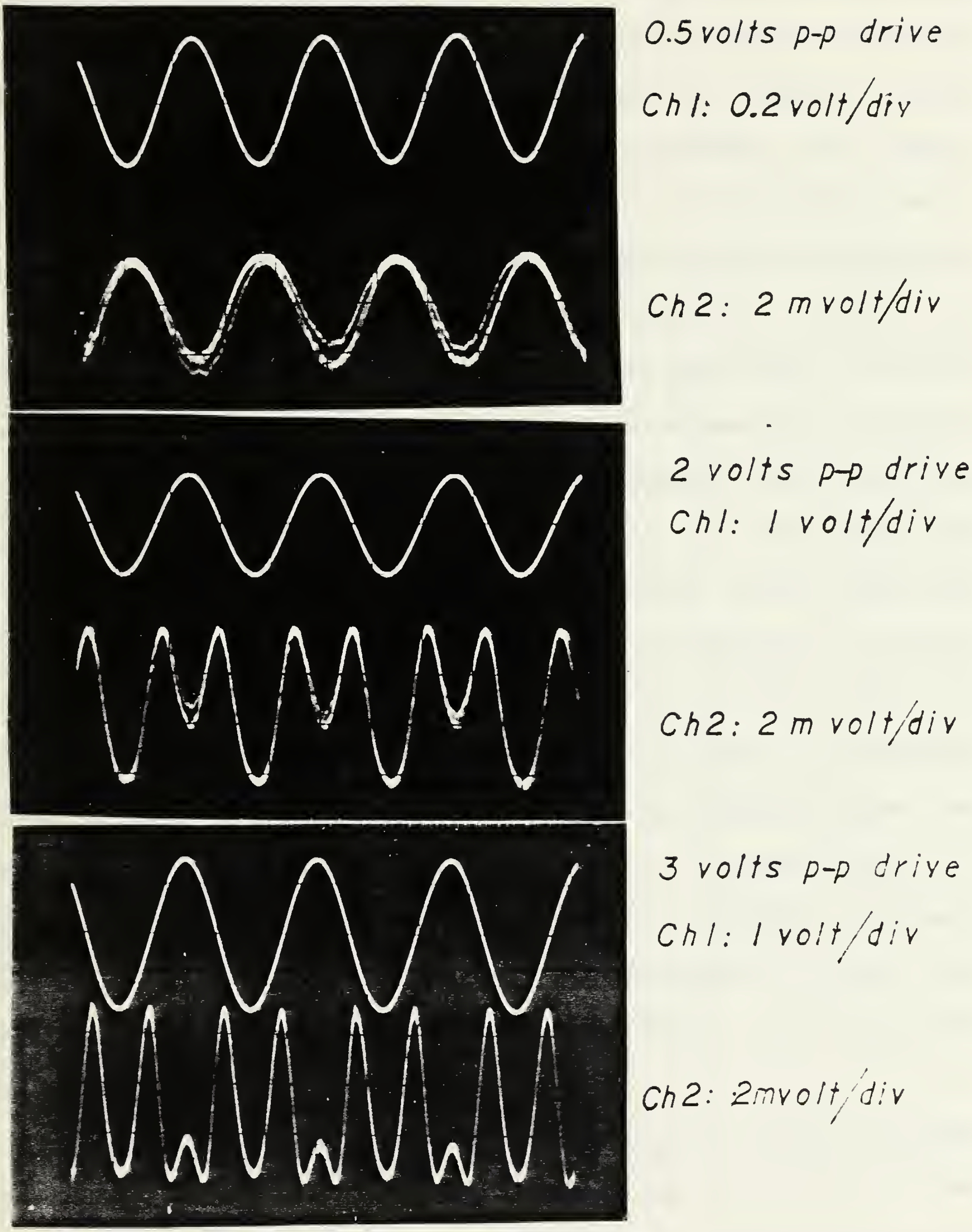

Figure 4.2 Oscillograms of PZT Drive Signal and Photodiode Output Signal

the prescribed settings. At the lower voltage amplitude limit the spectrum analyzer seeks for the maximum amplitude of the fundamental and first two harmonics attained during a selected period of time. The amplitude of these signals vary in time as the angle ϕ varies randomly. The sample time selected on the spectrum analyzer, of the order of 16 seconds, was sufficient that the actual maximum values were attained and recorded. The HP-85F computer directs the spectrum analyzer to output the maximum amplitude values of the fundamental and harmonics. These values are stored by the computer. The computer then directs the function generator to increase the drive voltage by the specified incremental value. The spectrum analyzer again seeks for the maximum amplitudes and the process is repeated. This is done for each incremental value until the upper limit is reached. The data stored in the computer memory is sent to the printer and also transferred to magnetic tape for permanent storage to enable analysis at a later time. A graph of the data is plotted on the computer printer. Sample of data obtained is seen in Appendix B. From this data plots of the type shown in Figure 4.3 could be generated.

The computer program was run initially with the CW-234 laser source. Three runs were made, two with the fiber wrapped PZT cylinder of one arm acting as the modulator and one with the other fiber wrapped PZT of the other arm.

After replacement of the source with the CWX-233 laser was accomplished two more runs were made, one on each PZT cylinder. From the data, the amplitude of the drive signal that causes the fundamental to be at its first null was determined to be 1.65V(peak)±0.04V(peak). Thus, referring to equation (4.1), it may be concluded that the drive condition was such that the first order Bessel function J_1 was at a zero. The first of the fundamental's zeroes occurs at a phase shift of $k_0 x = 3.83$ radians. Therefore for the 8 meters of fiber wrapped on the PZT cylinder a value of 0.29 rad/volt(peak)/meter results. By observing the drive voltages required to produce the first zero of the fundamental as the frequency was varied manually it was possible to determine that the phase shift per volt remained constant, within the precision of the measurements, for frequencies from 80 hertz to 1500 hertz.

Agreement of experimental data presented in Appendix B and illustrated in Figure 4.3 to Bessel function theory is shown in Table II. The ratio of experimental maxima and minima of the same harmonic are compared to the theoretical ratio of maxima and zeros of Bessel functions of the same order. Theoretical data as tabulated by Abramowitz and Stegun [Ref. 15] was used.

The last test conducted was to verify operation of the system with the locking circuit. After aligning the locking, a small amplitude sine wave was applied to one of

TABLE II

Comparison of Experimental Data with Bessel Theory

	Minima				Maxima			
Order n	Drive voltage at minimum of order n [volts (rms)]	Ratio of min volt. order n to min volt. order 1	Theoretical ratio of Bessel zero $j_{s,n} : j_{s,1}$	$\Delta\%$	Drive voltage at maximum of order n [volts (rms)]	Ratio of max volt. order n to max volt. order 1	Theoretical ratio of Bessel zero $j_{s,n} : j_{s,1}$	$\Delta\%$
Fundamental $s=1$								
1	1.19	1.00	1.00	0	0.549	1.00	1.00	0
2	2.19	1.84	1.83	0.5	1.64	2.99	2.9	3.1
3	3.18	2.67	2.66	0.6	2.7	4.9	4.7	4.2
1^{st} Harmonic $s=2$								
1	1.59	1.00	1.00	0	0.965	1.00	1.00	0
2	2.63	1.65	1.64	0.7	2.08	2.18	2.1	3.8
2nd Harmonic $s=3$								
1	1.98	1.00	1.00	0	-	-	-	-
2	3.04	1.54	1.53	0.7	-	-	-	-

the PZT cylinders simulating an acoustic signal. The locking circuit produced a signal, similar to this input signal, that was fed back to the PZT cylinder in the other arm to act as a compensation signal, thus maintaining the two arms in quadrature. This output signal from the locking circuit was also sent to the oscilloscope to show that the output signal did follow the input signal.

B. INDIVIDUAL SENSOR SENSITIVITY

The individual acoustic sensitivity of the sensor coils in each arm of the interferometer was calculated from measurements obtained in the acoustic calibrator. A single coil was mounted on a stand with an LC-10 hydrophone placed in the center of the coil as shown in Figure 4.4. The acoustic calibrator was driven at a frequency that generated a standing wave acoustic resonance. Chapter III section D7 discusses the standing waves generated in the calibrator. The coil/LC-10 hydrophone setup was lowered to the first maximum point of the standing wave. Output of one of the photodiodes of the interferometer was sent to the Tektronix 2215 oscilloscope and the HP-3582A spectrum analyzer. Output of the LC-10 hydrophone was sent to the HP-3438A Multimeter set to read AC voltage. A schematic of the instrumentation setup is shown in Figure 4.5. The spectrum analyzer was set to monitor the fundamental frequency and the first two harmonics. Drive voltage was increased to the

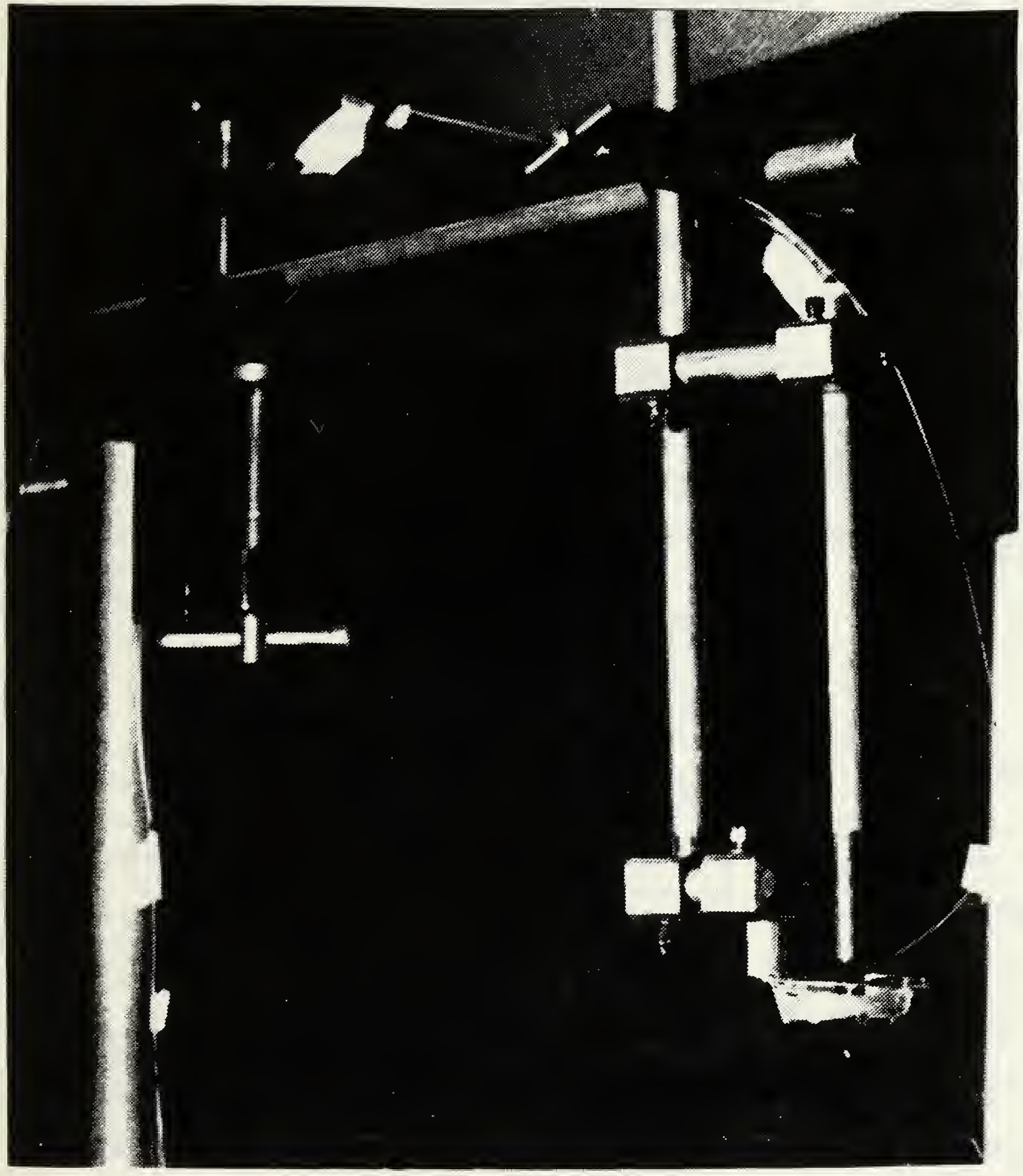

Figure 4.4 Photograph of LC-10 Hydrophone and Single Fiber Coil Setup

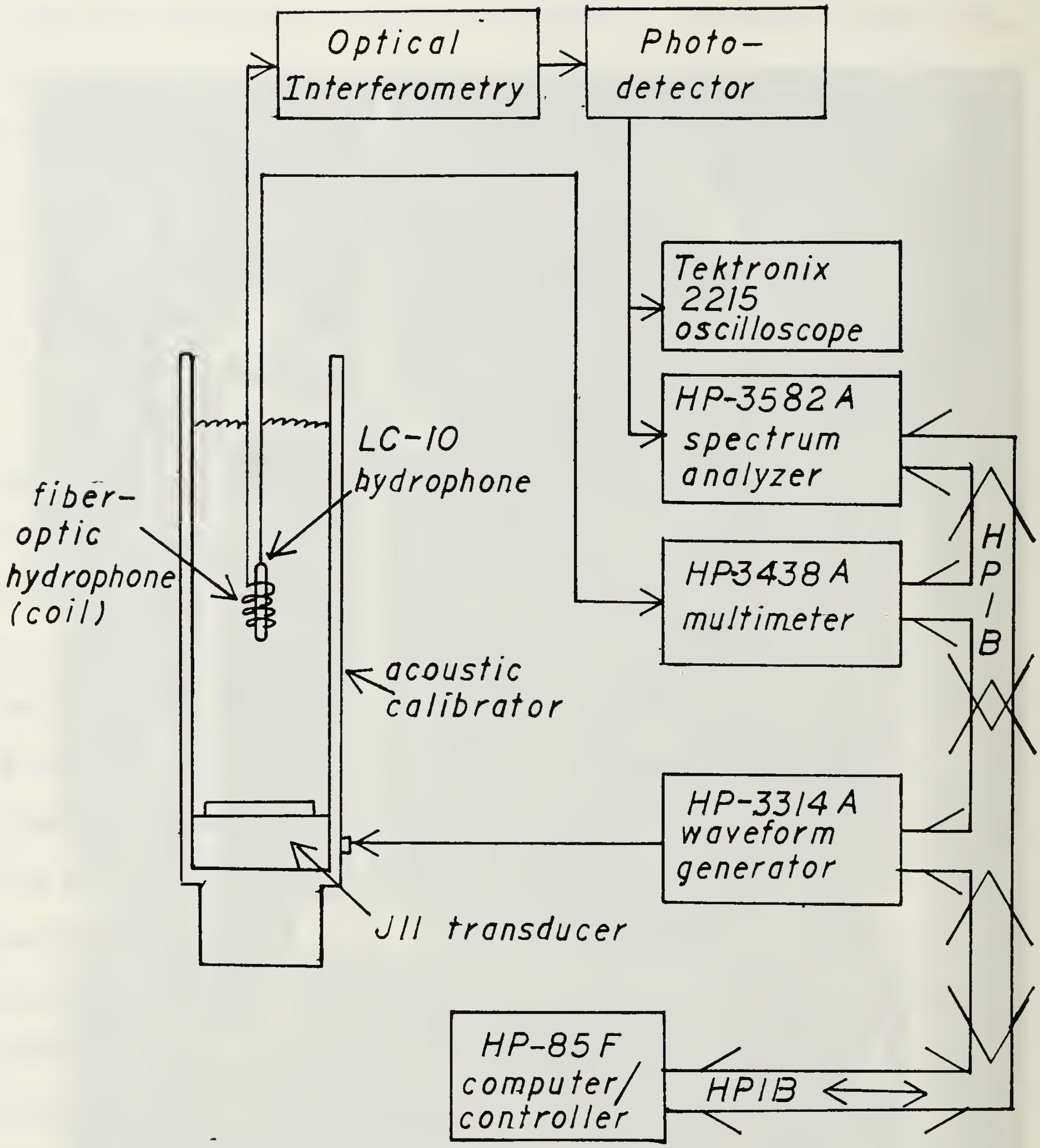
Optical Interferometry
Photo-detector
Tektronix 2215 oscilloscope
HP-3582 A spectrum analyzer
HP3438 A multimeter
HPIB
HP-3314 A waveform generator
HP-85 F computer/controller
HPIB
LC-10 hydrophone
fiber-optic hydrophone (coil)
acoustic calibrator
J11 transducer

Figure 4.5 Block Diagram of Calibration Circuit

acoustic calibrator until the voltage of the fundamental frequency, as seen on the spectrum analyzer, reached its first minimum value. The voltage of the LC-10 was recorded. If there was more than one pressure maximum the sensor arrangement was moved to the next pressure maximum and the LC-10 voltage at the fundamental's first zero point was recorded. Data were recorded for all of the pressure maxima of the standing wave. Data were obtained both manually and by computer control as discussed in the above section.

The first minimum of the fundamental occurs at a phase shift of 3.83 radians, therefore the sensitivity of the coil M_C in optical radians per micropascal is calculated as follows:

$$M_C = M_H * 3.83\text{rads}/V_H \tag{4.2}$$

where M_H is the sensitivity of the LC-10 hydrophone in volts/μPa obtained from manufacture specification sheets. V_H is the LC-10 hydrophone voltage where the first zero of the fundamental occurred. Table III is a summarization of all single coil sensitivity measurements taken at three different calibrator resonances and different depths associated with pressure maxima.

Table III

Individual Coil Sensitivity

Coil # 1					Coil # 2				
Freq (Hz)	Depth of Hyd from Air-Water Boundary (cm)	Nos. of Runs	Avg M $\frac{\mu rad}{\mu Pa}$ 10^{-3}	Std dev $\frac{\mu rad}{\mu Pa}$ 10^{-3}	Freq (Hz)	Depth of Hyd from Air-Water Boundary (cm)	Nos. of Runs	Avg M $\frac{\mu rad}{\mu Pa}$ 10^{-3}	Std dev $\frac{\mu rad}{\mu Pa}$ 10^{-3}
392	23	1	7.07	-	390	23	1	5.65	-
385	60	1	12.4	-	389	65	1	9.99	-
385	80	9	9.15	2.31	385	78	9	10.3	2.4
544*	16	6	4.95	.563	593	16	4	5.19	.314
593	48	7	8.66	1.14	593	48	3	11.5	.529
544	47	10	9.93	2.97	-	-	-	-	-
695*	12	9	9.77	2.41	704	11	13	8.45	1.36
695	37	5	10.4	.295	695	36	18	12.6	1.57
695	65.5	7	25.4	4.99	700	62.5	18	21.6	9.15
695	91.5	28	18.6	6.8	690	92.5	6	20.7	9.27

* Depth of water column changed from 93cm to 100cm to shift second resonance from 593 to 544 Hz, and to shift third resonance from 752 to 695 Hz.

If all of the measurements taken are grouped together neglecting frequency and coil position in the calibrator, the blind average of the sensitivities are:

$$\text{Coil \#1} \quad M_{C1} = 13.8 \times 10^{-3} \ \mu\text{rad}/\mu\text{Pa}$$

with a standard deviation of:

$$\sigma = 7.5 \times 10^{-3} \ \mu\text{rad}/\mu\text{Pa}$$

and

$$\text{Coil \#2} \quad M_{C2} = 13.9 \times 10^{-3} \ \mu\text{rad}/\mu\text{Pa}$$

with a standard deviation of:

$$\sigma = 7.7 \times 10^{-3} \ \mu\text{rad}/\mu\text{Pa}$$

As can be seen from Table III and the blind averages, the individual coil sensitivities are matched well within experimental error.

Table III indicates an increase in coil sensitivity as depth is increased with exception of very deep depths where proximity of the sensors to the source appears to have effected the measurements.

C. GRADIENT SENSOR SENSITIVITY

A gradient sensor was formed by placing the two fiber coils in the calibrator separated by a distance of 10 cm. The LC-10 hydrophone is placed in the center of the coils approximately 5 cm from each coil. The LC-10 hydrophone and both of the coils are then submerged in water and exposed to an acoustic field and an established acoustic pressure gradient. If the pressure sensitivities of the two coils are closely matched, the pair does not respond to the pressure, but to the spatial pressure gradient. Such a gradient sensor can be utilized to detect the direction of an incident acoustic wave as discussed under conventional gradient hydrophones in chapter II.

The J11 transducer source of the acoustic calibrator is driven at a frequency to produce a well defined standing wave. The LC-10 hydrophone/ dual coil setup is submerged to a location of a pressure minimum, defined as a point where the voltage from the LC-10 hydrophone is at a minimum. With the LC-10 at this position the two coils are located on either side of the pressure minimum and therefore in a region of maximum pressure gradient. The external instrumentation arrangement is the same as when individual coil sensitivities were obtained. The driver amplitude is increased until the amplitude of the fundamental frequency reaches its first zero point. However, the drive voltage, not the LC-10 voltage was recorded. Since the LC-10 hydrophone is at a minimum pressure position, its output voltage is quite low and, therefore, the pressure in the region of the coils could not be directly computed using just LC-10 sensitivity.

However, by knowing LC-10 voltage (V_H) at a pressure maximum for a set drive voltage a correlation between LC-10 voltage and J11 drive voltage could be calculated. Using LC-10 sensitivity (M_H), a value of pressure per J11 drive volts is obtained. This is shown in the following formula:

$$P_o/\text{J11volts} = [V_H \text{ at } P_{max}]/[M_H * \text{J11voltage}] \qquad (4.3)$$

Recall from Chapter II, equation (2.6), the pressure at a distance x above and below (+,−) a pressure minimum (assuming $x \ll \lambda$) is:

$$P_{\pm} = \pm P_o kx$$

(4.4)

Replacing P_o of equation (4.4) with equation (4.3) and multiplying by the drive voltage needed to reach the first zero of the fundamental (V_{J11}) the pressure at a distance x is:

$$P_{\pm} = [(P_o/\text{J11volts})*V_{J11}]kx$$

(4.5)

With the coils equally spaced on either side of the pressure minimum, the difference in pressure is twice the pressure at one of the coil locations. The pressure gradient is the pressure difference divided by the separation between the coils, and is given by the following formula:

$$\nabla P = 2P_{\pm}/\Delta x$$

(4.6)

Gradient sensitivity is calculated directly by the following formula, when the pressure gradient is sufficient to null the amplitude of the fundamental:

$$M_D = 3.83\text{rads}/\nabla P \tag{4.7}$$

The units of gradient sensitivity are radians/ μ Pa/cm.

Gradient sensitivity can also be calculated indirectly by using single coil sensitivity values. Indirect gradient sensitivity can be expressed as follows:

$$M_{ID} = \left(\phi_1 - \phi_2\right) / \nabla P \tag{4.8}$$

where ϕ_1 and ϕ_2 are the phase shifts in coil 1 and coil 2 respectively. Using the pressure value as expressed in equation (4.5) the phase shifts may be expressed as:

$$\phi_1 = P_+ * M_{C1} \tag{4.9}$$

and

$$\phi_2 = P_- * M_{C2} \tag{4.10}$$

where P_+ and P_- are the pressure amplitudes at the sensor coil locations and M_{C1} and M_{C2} are single coil sensitivities obtained from Table III. Inserting equations (4.9) and equation (4.10) into equation (4.8) and using the fact that $P_+ = -P_-$ when the sensor is at a pressure node, the indirect gradient sensitivity can be expressed as:

$$M_{ID} = P_{\pm}[M_{C1} + M_{C2}]/\nabla P \tag{4.11}$$

Substituting equation (4.6) into equation (4.11) results in an indirect gradient sensitivity formula as follows:

$$M_{ID} = [M_{C1} + M_{C2}]/[2/\Delta x] \tag{4.12}$$

where ΔX is the separation between the two coils and this distance is assumed to be smaller than a wavelength.

Table IV is a summary of direct and indirect gradient sensitivity measurements calculated from dual coil and single coil data respectively. Measurement of direct gradient sensitivity was calculated at three different calibrator resonances and different depths associated with pressure minima (maximum pressure gradient). Indirect gradient sensitivity is also calculated at three different calibrator resonances but uses the average sensitivity

TABLE IV

Gradient Sensor Sensitivities

Measured (dual coil data)										Calculated (single coil data)			
Freq (Hz)	No. of Runs	Hydrophone Depth (cm)	std dev (cm)	Avg $\frac{P_o}{J11V}$ $\frac{\mu Pa}{volts}$ X10^{7}	std dev $\frac{\mu Pa}{volts}$ X10^{7}	Avg J11 voltage at 1st zero of fund. freq (volts)	std dev volts	M_{grad} (direct) $\frac{\mu rad}{\mu Pa/cm}$ X10^{-2}	% experimental uncertainty	Freq (Hz)	Depth from Table III (cm)	M_{grad} (indirect) $\frac{\mu rad}{\mu Pa/cm}$ X10^{-2}	% experimental uncertainty
391	9	46.2	0.51	14.12	--	3.15	0.96	12.3	31	391	23	6.36	5
-	-	-	-	--	--	--	--	--	-	387	63	11.2	5
-	-	-	-	--	--	--	--	--	-	385	79	9.7	35
593	7	29.3	1.1	9.53	0.12	3.72	0.84	10.5	23	593	16	5.07	14
593	13	59.7	1.1	9.53	0.12	3.64	1.25	10.7	35	593	48	10.1	24
593	20	note 1	-	9.53	0.12	3.67	1.1	10.6	31	593	note 2	7.76	22
752	10	20.2	1.4	4.96	0.56	4.27	0.36	13.8	15	698	11.5	9.1	31
752	11	43.7	1.8	4.96	0.56	4.17	0.43	14.2	16	695	36.5	11.5	15
752	6	67.5	1.1	4.96	0.56	4.59	0.55	12.9	17	697	63	23.5	45
752	27	note 3	-	4.96	0.56	4.3	0.45	13.7	17	692	92	19.7	59

note 1: average of data at 29.3 and 59.7 cm
note 2: average of data at 16 and 48 cm
note 3: average of data at 20.2, 43.7, and 67.5 cm

obtained at a pressure maxima for the single coils divided by the desired distance between the coils (equation (4.12)).

Error analysis for direct gradient sensitivity can be made by taking the square root of the sum at squares of the constituents of equation (4.6). This may be expressed as follows:

$$\left(\frac{\partial M}{M}\right)_D = \left[\left(\frac{\partial \frac{P_o}{J11V}}{\frac{P_o}{J11V}}\right)^2 + \left(\frac{\partial V_{J11}}{V_{J11}}\right)^2 + \left(\frac{\partial c}{C}\right)^2 + \left(\frac{\partial x}{X}\right)^2\right]^{1/2} \tag{4.13}$$

where C is the experimental average speed of sound in the calibrator as shown in Table I. All other symbols are as explained in equation (4.3) and equation (4.5).

Error analysis for indirect gradient sensitivity may be expressed as follows:

$$\left(\frac{\partial M}{M}\right)_{ID} = \left[\left(\frac{\partial \langle \overline{M} \rangle}{\overline{M}}\right)^2 + \left(\frac{\partial x}{X}\right)^2\right]^{1/2} \tag{4.14}$$

where $\langle \overline{M} \rangle$ is the average deviation for single coil sensitivities and $\overline{M}$ is the average of the single coil sensitivities as presented in Table III.

D. ANALYSIS

A general analysis of single coil sensitivity compared to published data [Ref.6] can be shown. From Table III typical sensitivities are on the order of approximately

10^{-2} μrad/μPa per hydrophone for 10 meters of fiber. This results in a sensitivity of 10^{-3} μrad/μPa/m. For an optical wavelength of 0.83 microns, the experimental value of $\Delta\phi/\phi\Delta P$ is approximately 130×10^{-12} pascal^{-1}. For the same diameter fiber (0.4mm), the calculated value is greater than published values [Ref. 5] by a factor of four to five. This variation could be explained in terms of the large variations in observed physical properties of Hytrel coatings resulting in a more sensitive fiber.

As shown in Table III, the single coil sensitivities of coil 1 and coil 2 at the same depth appear to be closely matched within experimental error. The sensitivity of the individual coils are not matched over a depth range in the acoustic calibrator. The data indicates that the sensitivity of the single coil is a function of depth with possible near field effect occuring close to the source causing an anomaly. No reason could be found for this result but follow-on experiments will investigate this depth dependent sensitivity of single coils.

Measured pressure gradient sensitivity and calculated pressure gradient sensitivity as shown in Table IV in the previous section are in agreement within experimental error. The measured pressure gradient sensitivity obtained from data at pressure minima is shown to be more constant with frequency and depth than the calculated pressure gradient sensitivity based on single coil measurements at pressure maxima. Where the single coil data at Table III is a function of depth the measured sensitivity of the dual coil setup appears to be relatively independent of depth with an average value of 0.124±0.015 μrad/μPa/cm.

Final analysis of the pressure gradient hydrophone was conducted by connecting the output of the photodiodes to the phase-lock loop locking circuit. The dual fiber coils with a LC-10 hydrophone in the center was lowered in the acoustic calibrator. The voltage from the locking circuit and the LC-10 hydrophone were recorded. Figures 4.6 and 4.7 are plots of the recorded data at 593 Hz and 752 Hz respectively. As shown in Figures 4.6 and 4.7 as LC-10 hydrophone proceeds to a minimum gradient hydrophone voltage proceeds to a maximum and as LC-10 hydrophones proceeds to a maximum gradient hydrophone voltage proceed to a minimum. The data to produce Figures 4.6 and 4.7 is in good agreement with theory except for data recorded near the source or near the air-water boundary.

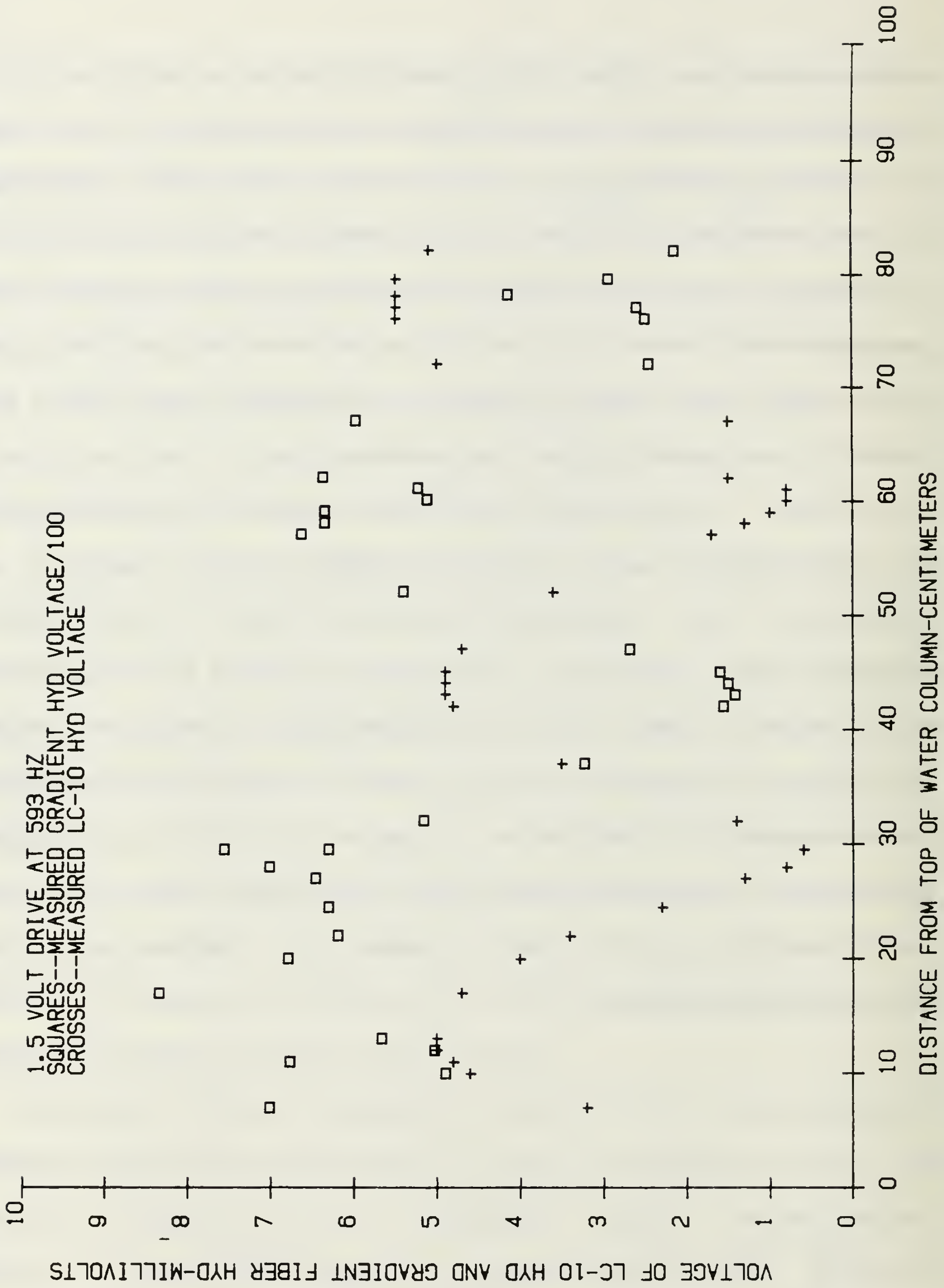

Figure 4.6 Demodulated Gradient Hydrophone Output at 593 Hz.

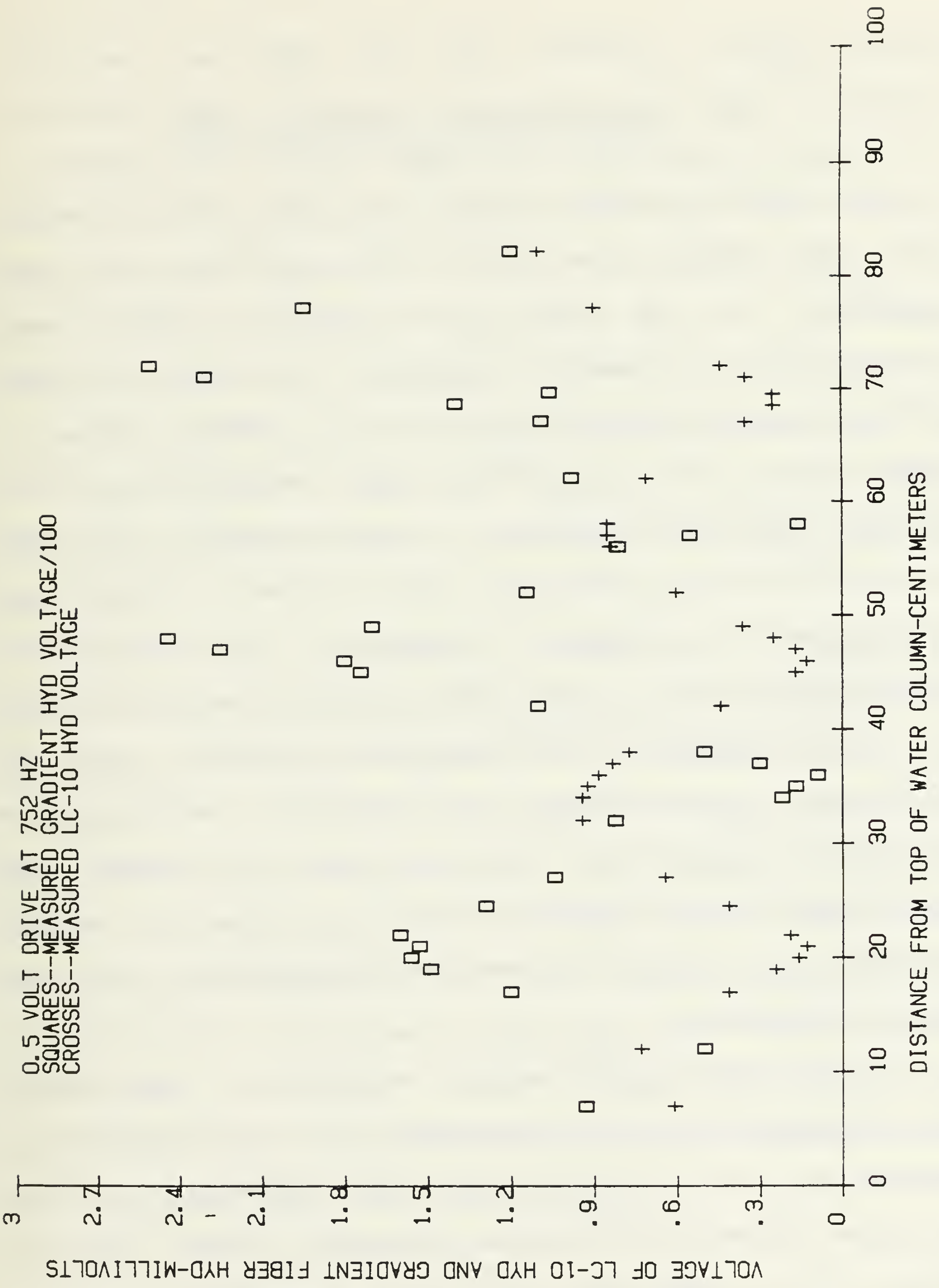

Figure 4.7 Demodulated Gradient Hydrophone Output at 752 Hz.

V. CONCLUSIONS AND RECOMMENDATIONS

Since their invention in the late 1970's [Ref. 3 and 4], many applications for fiber optic sensors have been suggested. In the area of low frequency (audio) sound transduction in the sea (hydrophones), it was felt the most reasonable application of this class of sensor was as a dipole sensor. The potentially high sensitivity could be exploited since the output of a dipole sensor is the small difference of two relatively large signals. Secondly, an interferometric (homodyne) detector is intrinsically differential since, in this case the interference is created by the difference of the optical path lengths in the two arms of the interferometer. An additional benefit of this differential operation is the high degree of common mode noise rejection which maybe gained by having the "sensor" and "reference" arm in the same environment until the very end of the sensor.

The laboratory investigations outlined in this report have demonstrated the feasibility of this application. Because the fiber optic system is essentially a phase modulated rather than amplitude modulated system (equation 2.22), it is difficult to make an absolute comparison between it and a piezoelectric pressure gradient sensor. Before the impedance converting, 20 dB gain, internal amplifier, the USRD type G63 standard pressure gradient hydrophone [Ref. 13] has a sensitivity of 7.5×10^{-9} V/μPa/cm. The fiber optic system described here using piezoelectric phase shifter (Chapter III section A-4) and the feedback locking circuit (Chapter III section D-8) had an output of 305±8 mV/radian (Chapter IV section A and Fig. 4.3). This combined with an average gradient sensitivity of 0.124±0.015 μrad/μPa/cm gives an overall sensitivity for the fiber system of $3.8\pm0.5\times10^{-8}$ V/μPa/cm. By this method, the fiber system has a 14 dB advantage over the USRD type G63.

At this stage, further work in this area is justified. The directions that should be pursued are the ruggedizing of the sensor, and the development of a package which will incorporate the sensor and couplers in a single submersible unit, possibly to be followed by the integration of the laser and demodulators in the same unit. Alternative demodulation schemes which do not require a piezoelectric fiber stretcher to maintain "quadrature lock" should also be investigated. Finally, direct comparison with other directional dipole sensors such as those on DIFAR sonobuoys should be made under real sea conditions.

APPENDIX A

DATA ACQUISITION PROGRAM

This program was written to use a HP-85F computer to gather data more accurately and quickly than by manual means. This program was used after initial construction and prior to sensitivity experiments to obtain data for computation of interferometer characteristics (see Figure 4.1). Chapter IV Section A gives a detailed explanation of how this program was utilized for computerized data acquisition.

```
 10 OPTION BASE 1
 20 SHORT F(3), A(250), B(250,3), C(250,3), E(250)
 30 REM ** OBTAIN INITIAL VALUES FOR PARAMETERS **
 40 DISP "ENTER FUND FREQ"
 50 INPUT F(1)
 60 DISP "ENTER SPECT ANAL START FREQ"
 70 INPUT F1
 80 DISP "ENTER START AMPLITUDE IN MVOLTS"
 90 INPUT A(1)
100 DISP "ENTER END AMPLITUDE IN MVOLTS"
110 INPUT V1
120 DISP "ENTER INCREMENT VALUE IN MVOLTS"
130 INPUT I
140 F(2)=2*F(1)
150 F(3)=3*F(1)
160 REM ** PRESET AND INITIALIZE HP-3314 AND HP-3582 **
170 OUTPUT 707 ;"PR"
180 OUTPUT 707 ;"FR",F(1),"HZAP,A(1),"MVFU1"
190 OUTPUT 711 ;"PRS"
200 OUTPUT 711 ;"AS8SL1MN1MD4SP10AD",F1,"SC1AV4NU4AM2"
210 J=(V1-A(1))/I+1
220 REM ** DATA ACQUISITION FOR SET DRIVE AMPLITUDE **
230 FOR R=1 TO J
240 OUTPUT 711 ;"RE"
250 WAIT 11500
260 ENTER 723 ; V
270 E(R)+V
280 REM ** STORE AMPLITUDE OF FUND AND 1ST TWO HARMONICS **
290 FOR N=1 TO 3
300 M=(F(N)-F1)/1000*250
310 OUTPUT 711 ;"MP",M
320 OUTPUT 711 ;"LMK"
330 ENTER 711 ; B(R,N),C(R,N)
340 NEXT N
350 D=R+1
360 A(D)=A(R)+I
370 OUTPUT 707 ;"AP",A(D),"MV"
380 NEXT R
390 REM ** OUTPUT DATA TO PRINTER **
400 PRINTER IS 701,80
410 PRINT "FUND FREQ (HZ) =",F(1)
420 PRINT 'SOURCE VOLTS     LC10"
430 PRINT "MILLIVOLTS(P-P) VOLTS(RMS) VF1(RMS) VF2(RMS)
    VF3(RMS)"
440 FOR R=1 TO J
450 IMAGE 50,12X,D.DDE,4X,D.DDE,4X,D.DDE,4X,D.DDE
460 PRINT USING 400 ; A(R),E(R),B(R,1),B(R,2),B(R,3)
```

```
470 NEXT R
480 REM ** RESET INSTRUMENTATION TO PRESET CONDITION **
490 OUTPUT 707 ;"PR"
500 OUTPUT 711 ;"PRS"
510 REM ** STORE DATA ON TAPE **
520 ASSIGN# 1 TO "HYD1"
530 PRINT# 1,1 ; A()
540 PRINT# 1,2 ; E()
550 PRINT# 1,3 ; B(,)
560 ASSIGN# 1 TO *
570 REM ** PLOT DATA ON COMPUTER PRINTER **
580 PRINTER IS 2
590 FOR K=1 TO 3
600 GCLEAR
610 SCALE 0,10000,0,.01
620 XAXIS 0,1000
630 YAXIS 0,.001
640 PENUP
650 FOR I=1 TO J
660 PLOT A(I),B(I,K)
670 NEXT I
680 COPY
690 NEXT K
700 GCLEAR
710 SCALE 0,10000,0,.01
720 XAXIS 0,1000
730 YAXIS 0,.001
740 FOR K=1 TO 3
750 PENUP
760 FOR I=1 TO J
770 PLOT A(I),B(I,K)
780 NEXT I
790 NEXT K
800 COPY
810 DISP "END"
820 END
```

APPENDIX B

SAMPLE RAW DATA

PZT #1

Laser Diode Current 35 milliamps

Fundamental frequency (Hz) 372

Source Voltage (volts) (rms)	Fundamental Voltage (millivolts) (rms)	1st Harmonic Voltage (millivolts) (rms)	2nd Harmonic Voltage (millivolts) (rms)
0.035	0.783	0.030	0.0019
0.053	1.180	0.066	0.0039
0.071	1.570	0.105	0.0048
0.071	1.980	0.182	0.0106
0.089	2.320	0.239	0.0164
0.106	2.700	0.349	0.0241
0.124	3.050	0.456	0.0347
0.142	3.430	0.544	0.0473
0.159	3.800	0.642	0.0647
0.177	4.070	0.812	0.0830
0.195	4.380	0.916	0.1150
0.230	4.820	1.130	0.1460
0.247	5.010	1.270	0.1720
0.247	5.340	1.510	0.2060
0.265	5.590	1.610	0.2540
0.283	5.790	1.750	0.2880
0.300	6.110	2.010	0.3280
0.318	6.310	2.150	0.4070
0.336	6.460	2.370	0.4520
0.353	6.850	2.440	0.5200
0.373	6.870	2.460	0.5770
0.390	7.130	2.960	0.6490
0.409	7.240	2.970	0.7160
0.426	7.330	3.320	0.8160
0.444	7.370	3.420	0.8880
0.461	7.550	3.630	0.9650
0.478	7.700	3.830	1.0500
0.497	7.750	3.990	1.1300

0.513	7.650	4.070	1.2600
0.532	7.750	4.320	1.3100
0.549	7.890	4.250	1.4400
0.567	7.460	3.990	1.5000
0.584	7.730	4.690	1.6700
0.603	7.770	4.360	1.7400
0.620	7.650	5.030	1.8100
0.638	7.450	4.720	1.9400
0.655	7.460	5.190	2.0200
0.672	7.350	4.910	2.2200
0.691	7.280	5.080	2.2900
0.707	7.070	5.450	2.4000
0.726	6.930	5.460	2.5400
0.743	6.850	5.650	2.6700
0.761	6.590	5.730	2.8100
0.778	6.500	5.820	2.9500
0.797	6.200	5.970	3.0400
0.814	6.050	6.050	3.1800
0.832	5.760	6.100	3.2900
0.849	5.550	6.320	3.3600
0.868	5.290	6.230	3.4900
0.885	5.070	6.370	3.6100
0.902	4.770	6.500	3.6900
0.920	4.490	6.480	3.8500
0.937	4.200	6.540	4.0000
0.956	3.870	6.540	4.0600
0.973	3.590	6.480	4.1900
0.991	3.270	6.480	4.2200
1.010	3.000	6.560	4.4500
1.030	2.710	6.500	4.5600
1.040	2.360	5.910	4.6200
1.060	2.040	6.210	4.7300
1.080	1.750	6.170	4.7200
1.100	1.480	6.120	4.8400
1.110	1.170	6.070	4.8200
1.130	0.858	5.550	5.0100
1.150	0.617	5.630	5.1200
1.170	0.346	5.460	5.0600
1.190	0.339	5.320	5.1600
1.200	0.611	5.150	5.2500
1.220	0.841	4.840	5.2900
1.240	1.080	4.710	5.2800
1.260	1.390	4.570	5.2900
1.270	1.610	4.280	5.2800
1.290	1.920	4.050	5.2900
1.310	2.170	3.630	5.3600
1.330	2.370	3.560	5.4000
1.340	2.600	3.370	5.3400
1.360	2.830	3.070	5.2500
1.380	2.980	2.840	5.2500
1.400	3.260	2.660	5.1900

1.420	3.340	2.410	5.1400
1.430	3.540	2.210	5.0500
1.450	3.620	1.930	4.8700
1.470	3.900	1.780	4.9600
1.490	3.930	1.500	4.8100
1.500	4.110	1.310	4.7100
1.520	4.200	1.080	4.5800
1.540	4.230	0.863	4.4800
1.560	4.360	0.583	4.3900
1.570	4.440	0.366	4.2700
1.590	4.510	0.293	4.1200
1.610	4.560	0.345	3.9900
1.630	4.530	0.601	3.8100
1.640	4.410	0.766	3.6000
1.660	4.560	1.020	3.4900
1.680	4.530	1.220	3.3400
1.700	4.460	1.420	3.1300
1.720	4.350	1.580	2.9800
1.730	4.250	1.780	2.7600
1.750	4.250	1.930	2.5800
1.770	4.160	2.090	2.4400
1.790	4.010	2.290	2.2300
1.800	3.920	2.480	2.0300
1.820	3.890	2.720	1.8400
1.840	3.780	2.890	1.6600
1.860	3.670	3.020	1.4400
1.870	3.530	2.880	1.2600
1.890	3.210	3.370	1.0400
1.910	3.230	3.640	0.8710
1.930	3.030	3.630	0.6390
1.950	2.820	3.730	0.4490
1.960	2.570	3.860	0.2430
1.980	2.260	3.570	0.0772
2.000	2.320	3.990	0.1690
2.030	2.090	3.980	0.3640
2.050	1.940	4.080	0.5500
2.070	1.710	4.010	0.7450
2.080	1.510	4.120	0.9230
2.100	1.270	4.110	1.1200
2.120	1.090	4.050	1.2800
2.140	0.866	4.030	1.4200
2.150	0.683	3.960	1.6300
2.170	0.474	3.830	1.7800
2.190	0.320	3.880	1.9200
2.210	0.361	3.820	2.0700
2.210	0.524	3.760	2.1900
2.230	0.667	3.640	2.3500
2.240	0.909	3.370	2.4300
2.260	1.080	3.350	2.5400
2.280	1.260	3.220	2.7100
2.300	1.470	3.090	2.7800

2.310	1.640	2.960	2.9000
2.330	1.830	2.810	3.0400
2.350	1.990	2.690	3.0900
0.370	1.970	2.520	3.0700
2.380	2.190	2.370	3.1900
2.400	2.430	2.160	3.2100
2.420	2.570	2.010	3.3000
2.440	2.700	1.870	3.3200
2.460	2.790	1.740	3.3600
2.470	2.900	1.540	3.3400
2.490	0.950	1.390	3.2900
2.510	3.130	1.210	3.3700
2.530	3.180	1.030	3.3400
2.540	3.180	0.766	3.3100
2.560	3.270	0.678	3.3100
2.580	3.430	0.452	3.3000
2.600	3.380	0.320	3.1600
2.610	3.430	0.259	3.1000
2.630	3.430	0.253	3.0500
0.650	3.450	0.292	3.0500
2.670	3.430	0.438	2.9700
2.680	3.390	0.586	2.8700
2.700	3.490	0.800	2.7700
2.720	3.470	0.939	2.6800
2.740	3.390	1.160	2.5200
2.760	3.320	1.260	2.4300
2.770	3.310	1.510	2.3200
2.790	3.190	1.620	2.2100
2.810	3.130	1.820	2.0500
2.830	3.050	1.970	1.9100
2.840	2.970	2.130	1.7800
2.860	2.870	2.260	1.6500
2.880	2.740	2.350	1.4800
2.900	2.620	2.540	1.3400
2.920	2.510	2.600	1.1900
2.930	2.390	2.720	1.0500
2.950	2.270	2.780	0.8880
2.970	2.130	2.910	0.7160
2.990	1.990	3.000	0.5690
3.000	1.790	3.020	0.3920
3.020	1.690	3.100	0.2460
3.040	1.520	3.070	0.0733
3.060	1.360	3.070	0.0791
3.070	1.200	3.250	0.2470
3.090	0.997	3.250	0.3600
3.110	0.855	3.220	0.5340
3.130	0.686	3.220	0.6920
3.140	0.558	3.130	0.8300
3.160	0.404	3.100	0.9820
3.180	0.303	3.070	1.1300
3.200	0.454	3.020	1.2800

3.210	0.585	3.000	1.4000
3.230	0.748	2.720	1.5200
3.250	0.904	2.860	1.6400
3.270	1.030	2.640	1.7800
3.290	1.210	2.680	1.8700
3.300	1.330	2.520	1.9500
3.320	1.480	2.420	2.0400
3.340	1.550	2.330	2.1500
3.350	1.730	2.150	2.1800
3.370	1.870	2.070	2.3100
3.390	1.990	1.940	2.3500
3.410	2.130	1.850	2.4500
3.430	2.270	1.710	2.5300
3.440	2.330	1.560	2.5400
3.460	2.490	1.410	2.6400
3.480	2.470	1.280	2.6000
3.500	2.260	1.130	2.6500
3.520	2.650	0.984	2.6300

LIST OF REFERENCES

1. Cherin, A.H., An Introduction to Optical Fibers, McGraw-Hill, New York, 1983

2. Giallorenzi, T.G., Bucaro, J.A., Dandridge, A., Siegel, G.H., Cole, J.H., Rashleigh, S.C., Priest, R.G., "Optical Fiber Sensor Technology", IEEE Journal of Quantum Electronics, v. Q.E.-18, p. 626, 1982

3. Bucaro, J.A., Dardy, H.D., and Carome, E.F., "Fiber-Optic Hydrophone", Journal of the Acoustical Society of America, v. 62, p. 1302, 1977

4. Cole, J.H., Johnson, R.L., Bhuta, P.G., "Fiber-Optic Detection of Sound", Journal of the Acoustical Society of America, v. 62, p. 1136, 1977

5. Bucaro, J.A., Lagakos, N., Cole, J.H., Giallorenzi,T.G., "Fiber Optic Acoustic Transduction", Physical Acoustics Volume XVI, edited by Mason, W.P., Thurston, R.N., p. 385, Academic Press, 1982

6. Davis, C.M., Carome, E.F., Weik, M.H., Ezekiel, S., Einzig, R.E., Fiberoptic Sensor Technology Handbook, Dynamic Systems, Inc., McLean, Va., 1982

7. Bobber, R.J., Underwater Electroacoustic Measurements, Naval Research Laboratory, 1970

8. Carome, E.F., Satyshur, M.P., Acoustically Induced Phase and Intensity Modulation in Optical Fibers, John Carroll Univ., Dept. of Physics, Technical Report PH 78-2, 1978

9. Fritsch, K., Adamovsky, G., "Simple Circuit for Feedback Stabilization of a Single-Mode Optical Fiber Interferometer", Review of Scientific Instruments, v. 52, p. 996, 1981

10. Jackson, D.A., Priest, R., Dandridge, A., Tveten, A.B., "Elimination of Drift in a Single Mode Optical Fiber Interferometer Using a Piezoelectrically Streched Coiled Fiber", Applied Optics, v. 19, p. 2926, 1980

11. Lefevre, H.C., "Single-Mode Fiber Fractional Wave Devices and Polarization Controllers", _Electronics Letters_, v. 16, p. 778, 1980

12. Mills, G.B., Odero, D., "Reciprocity Calibration of a Transducer", Report for Transducer Acoustics Laboratory, Naval Postgraduate School, Dept. of Physics, 19 April 1983, (Unpublished)

13. Ivey, L.E., et al, _Underwater Electroacoustic Standard Transducers Catalogue_, Underwater Sound Reference Detachment, Naval Research Laboratory 1982

14. Schloss, F., Strasberg, M., "Hydrophone Calibration in a Vibrating Column of Liquid", _Journal of the Acoustical Society of America_, v. 34, p. 958, 1962

15. Abramowitz, M., Stegun, I.A., _Handbook of Mathematical Functions with Formulas, Graphs, and Mathematical Tables_, U.S. Dept. of Commerce, National Bureau of Standards, Tenth Printing, 1972

BIBLIOGRAPHY

Kinsler, L.E., Frey, A.R., Coppens, A.B., Sanders, J.V., Fundamentals of Acoustics, Wiley, New York, 1982.

LeBlanc, C.L., Handbook of Hydrophone Element Design Technology, NUSC Technical Document 5813 of 11 October 1978.

Urick, R.J., Principles of Underwater Sound, McGraw-Hill, New York, 1975.

Yariv, A., Optical Electronics, Holt,Rinehart and Winston, New York, 1976.

INITIAL DISTRIBUTION LIST

No. Copies

1. Defense Technical Information Center 2
Cameron Station
Alexandria, VA 22314

2. Library, Code 0142 2
Naval Postgraduate School
Monterey, CA 93943

3. Prof. E.F. Carome 8
Department of Physics (code 61 Cm)
Naval Postgraduate School
Monterey, CA 93943

4. Prof. S.L. Garrett 8
Department of Physics (code 61 Gx)
Naval Postgraduate School
Monterey, CA 93943

5. Prof. O.B. Wilson 1
Department of Physics (code 61 Wl)
Naval Postgraduate School
Monterey, CA 93943

6. Dr. L.E. Hargrove 1
Physics Division (code 412)
Office of Naval Research
800 N. Quincey St.
Arlington, VA 22217

7. Prof. J. Powers 1
Department of Electrical Engineering
(code 62 Po)
Naval Postgraduate School
Monterey, CA 93943

8. Commanding Officer 1
Underwater Sound Reference Detachment
Naval Research Laboratory
ATTN: T. Ruggerio
P.O. Box 8337
Orlando, FL 32856

9. LT G.B. Mills 2
95 Osprey Dr.
Groton, CT 06340

10. Chairman, Department of Physics (code 61) 1
Naval Postgraduate School
Monterey, CA 93943

11. Mr. Peter Rodgers - Code 425 UA 1
Project Manager - Underwater Acoustics
Office of Naval Research
800 N. Quincey St.
Arlington, VA 22217

12. Dr. M.E. Cole 1
Sohio Research Center
4440 Warrensville Center Rd.
Cleveland, OH 44128

13. Mr. & Mrs. G.B. Mills 1
1213 El Sur Way
Sacramento, CA 95825

14. Mr. J. Keane 1
Naval Air Development Center
Warminster, PA 18974

15. Mr. M. Seiman 1
Litton Guidance and Control Systems
5500 Canoga Ave.
Woodland Hills, CA 91365

16. Dr. Lyle Pauer 1
Goodyear Aerospace Corp.
Plant D
1210 Massilon Rd.
Akron OH 44315

17. Dr. H.J. Shaw 1
Ginzton Laboratory
Stanford University
Stanford, CA 94305

18. Mr. & Mrs. A.S. Fisher 1
5033 Cypress Ave.
Carmichael, CA 95608

19. Dr. C. Fritsch 1
Department of Physics
John Carroll University
Cleveland, OH 44118

20. Dr. J.A. Bucaro 1
Naval Research Laboratory
Code 5130
Washington D.C. 20375

21. Mr. & Mrs. M. Soloman 1
42 Marina Grande Court
Sacramento CA 95831

22. LT B.R. Ogg 1
135 Autumn Dr.
Strafford, VA 22554

23. Ron Mitnick 1
ELEX - Code 6121A
Naval Electronics Systems Command
Washington, D.C. 20363

24. CDR Richard M. Bostian 1
Naval Electronics Systems Command
PDE 120-113
Washington, D.C. 20363

25. LT Glen Macdonald 1
C/O Physics Dept. Code 61
Naval Postgraduate School
Monterey, CA 93943

26. CDR Kirk Evans 1
Defense Advanced Research Projects Agency
1400 Wilson Blvd.
Arlington, VA 22209

27. Mr. Robert J Baumbick 1
Mail Stop 100 - 1
Lewis Research Center
NASA
Cleveland, OH 44135

28. Mr. Thomas Higbee 1
ELEX - Code 6122
Naval Electronics Systems Command
Washington, D.C. 20363

602-197

207187

Thesis
M5943 Mills
c.1 Fiber optic gradient
hydrophone.

207187

Thesis
M5943 Mills
c.1 Fiber optic gradient
hydrophone.

thesM5943
Fiber optic gradient hydrophone.
3 2768 001 89074 2
DUDLEY KNOX LIBRARY